(1)

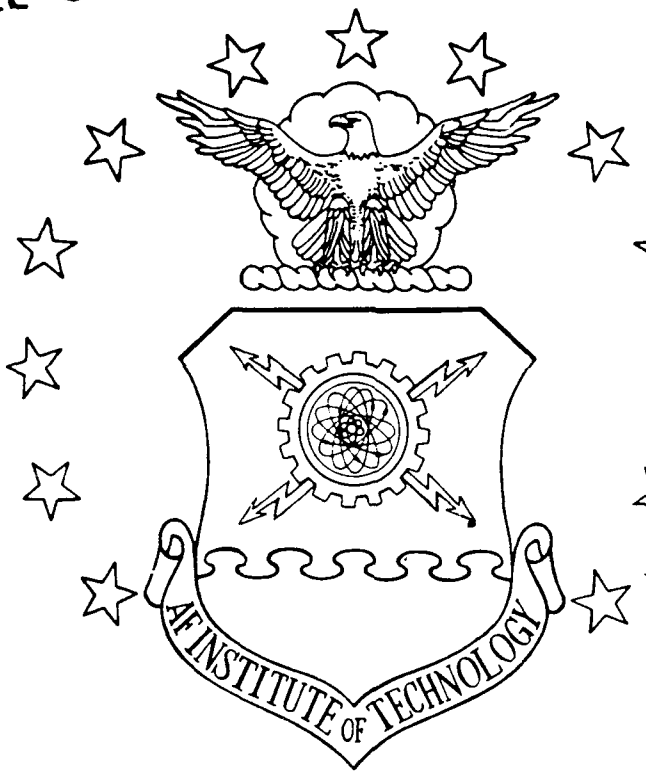

INVESTIGATION OF FAILURE MODES IN A CERAMIC COMPOSITE UNDER OFF-AXIS LOADING

THESIS

Walter E. Fink III
Captain, USAF

AFIT/GAE/ENY/89D-9

DEPARTMENT OF THE AIR FORCE
AIR UNIVERSITY
AIR FORCE INSTITUTE OF TECHNOLOGY

Wright-Patterson Air Force Base, Ohio

AFIT/GAE/ENY/89D-9

INVESTIGATION OF FAILURE MODES IN A CERAMIC COMPOSITE UNDER OFF-AXIS LOADING

THESIS

Presented to the Faculty of the School of Engineering

of the Air Force Institute of Technology

Air University

In Partial Fulfillment of the

Requirements for the Degree of

Master of Science in Aeronautical Engineering

Walter E. Fink III
Captain, USAF

December 1989

Preface

The purpose of this study was to investigate the off-axis behavior of a model ceramic composite (Corning's Nicalon/CAS II). Presently the ceramic composites are receiving a great deal of attention for use in structural applications.

Six different orientations (0, 15, 30, 45, 60, and 90 degrees) of the unidirectional material were tested in tensile loading. These tests results were compared with the existing theoretical modeling techniques for composite material behaviors. Although there was a limited amount of material, the test results correlated well with the existing modeling techniques commonly used for composites.

Throughout the experimentation and writing of this thesis I have had a great deal of help from others. I wish to acknowledge the great help by my advisor, Dr. Shankar Mall. Without his help this would not have been a delightful experience. Also, I wish to thank Ron Trejo and Dr Ran Kim of University of Dayton Research Center for there assistance and cooperation during the experimental part of my endeavor. Finally, I wish to thank my wife Tracy and son Wally for their understanding and cooperation during the time it took to complete this work.

Walter E. Fink III

Table of Contents

List of Figures

List of Tables

List of Symbols

Symbol	Definition
E_1	Principal direction axial modulus of elasticity for the composite
E_2	Principal direction transverse modulus of elasticity for the composite
G_{12}	Shear Modulus for the composite
ν_{12}	Poisson's Ratio in the principal direction for the composite
E_x	Off-axis load direction modulus of elasticity for the composite
E_y	Off-axis perpendicular to load modulus of elasticity for the composite
ν_{xy}	Poisson's Ratio in the off-axis coordinate system
E_m	Modulus of elasticity for the matrix
G_{12m}	Shear modulus for the matrix
ν_{12m}	Poisson's ratio for the matrix
E_f	Modulus of elasticity for the fiber
ν_{12f}	Poisson's ratio for the fiber
E_{2m}	Transverse modulus of elasticity for the matrix
E_{2f}	Transverse modulus of elasticity for the fiber
σ	Applied stress
σ_{xy}^{ult}	Off-axis ultimate stress
σ_{1m}^{ult}	ultimate stress of the matrix
σ_1	principle direction (fiber) applied stress
σ_2	principle transverse applied stress
σ_x	off-axis applied stress
$\Delta\sigma_o$	Incremental stress carried by the fibers after matrix cracking
ζ	Fiber packing geometry factor
V_f	Fiber volume fraction
V_m	Matrix volume fraction
τ'	Limiting shear stress
r	Fiber radius
2R	Center to center distance between fibers
X	Failure strength in fiber direction
Y	Failure strength in transverse direction
S	Shear strength
θ	Angle off-axis
ϵ_1	principle direction (fiber) strain

ε_2	principle transverse strain
ε_x	off-axis strain in load direction
ε_y	off-axis strain in transverse direction
ε_x^{ult}	off-axis ultimate strain in load direction
ε_y^{ult}	off-axis ultimate strain in transverse direction
ε_2^{mc}	principle transverse matrix cracking strain
ε_x^{mc}	off-axis matrix cracking strain in load direction
ε_y^{mc}	off-axis matrix cracking strain in transverse direction
cs	crack spacing

Abstract

The purpose of this study was to investigate the failure behavior of a ceramic composite (Corning's Nicalon/CAS II) under off-axis loading. The major objectives were to (1) investigate the initiation and propagation of damage mode due to off axis tensile loading and (2) compare present test results with the available material behavior modeling techniques for polymeric composites.

The specimens were tested in tension on an MTS test stand. Six different orientations (0, 15, 30, 45, 60, and 90 degrees off axis), with three specimens at each orientation, were tested. The 0, 15, 30, and 45 degree specimens were tested using the MTS grips. The 60 and 90 degree specimens were tested by gluing them into a fixture that had already been installed into the grips. At least one specimen with each orientation was tested to its ultimate failure point. Thereafter, other specimens were tested incrementally, stopping along the way, to find when and where matrix cracking starts. Acoustic emission was used to determine when cracking starts and replication was used to confirm the cracking.

The 0, and 15 degree specimens started cracking in the matrix during the linear portion of the stress-strain curve, at about 35 percent of their ultimate strengths. The 45

degree stress-strain curve had two linear and two nonlinear portions. The 45 degree specimen probably cracked at the onset of the first non-linear part of the stress-strain curve, although this has not been verified. The rest of the orientations cracked when they reached the ultimate strength. All off-axis load orientations broke parallel to the direction of the fiber, except the 15 degree which was 25 degrees off-axis. The 0 degree specimen showed a decrease in transverse strain before final failure occurred.

The test results showed that the Tsai-Hill failure criteria can approximate the ultimate failure stress and matrix cracking stress for this material in off-axis loading. The present modeling techniques for E_x and ν_{xy} will predict a trend for these values for this material. Although there was a large variance in data, the average values of E_x and ν_{xy} were close to the predicted values. The measured E_1 was in good agreement with its predicted value using the rule of mixtures. But E_2 was found to be in between the values obtained from the Halpin-Tsai equation (assuming a perfect elastic bonding between the fiber and matrix) and the modified Halpin-Tsai equation (assuming no bonding between the fiber and matrix).

This material should be tested at elevated temperature. Also, the effects of gage length of off-axis strength should be investigated. And finally, a theory needs to be developed to predict the onset of matrix cracking.

INVESTIGATION OF FAILURE MODES IN A CERAMIC COMPOSITE UNDER OFF-AXIS LOADING

I. Introduction

The need for high temperature, high strength materials is increasing because of developments of new high output engines and hypervelocity aircraft. Many ceramics and glasses possess high strength at high temperatures. But, they display low fracture toughness. A method of increasing the toughness of the ceramic or glass is to reinforce it with a high strength fiber. Fiber reinforced ceramic matrix materials usually consists of strong fibers surrounded by a weaker matrix to protect the fibers, bind the fibers together and transfer the load between the fibers. Because of the directionality of the matrix-fiber arrangement the material is no longer isotropic like most homogeneous materials. This makes the prediction of ceramic composites mechanical properties more complicated. A thorough understanding of a composites properties is essential for their use in critical structural areas. These materials could be useful in high strength environments which may include load in off-axis direction with respect to the fiber direction. The mechanical properties and failure initiation

of ceramic composites is not well understood. The failure of a fiber-reinforced material is partly due to the transfer of stress between the fiber and matrix. Kim and Pagano (1) showed matrix cracking occurs in the linear portion of the stress-strain curve. This transfer can be effected by the direction of orientations of the fiber to the tensile load. Also, different failure modes may be possible under off-axis loading of ceramic composites. There is an obvious need to understand these behaviors.

This study was therefore undertaken to understand how the material properties and failure modes of a ceramic composite are effected by off-axis loading. For this purpose, a model ceramic composite (Nicalon/CASII) manufactured by Corning Glass Works was selected. Nicalon is a silicon carbon fiber (SiC) commonly used in ceramic composites. CAS is a calcium aluminosilicate ceramic matrix developed by Corning Glass Works.

A. Background

Recently Nicalon/CAS II has been investigated in several studies. Kim and Pagano (1) looked at initiation of damage in unidirectional Nicalon/CAS II under tensile loading. They found matrix cracking starts in the linear portion of the stress-strain curve. Daniel, Anastassopoulos and Lee (2), saw the same effects. Also, Daniel et al showed the composite would continue to develop matrix cracks

until a certain crack density is reached, then the fibers would begin to fail. They also showed the matrix-fiber interface does have some bonding properties where some ceramic composites such as SiC/LAS (3) show no chemical bonding properties in the matrix-fiber interface and friction is the main method of transfer of load from matrix to fiber.

B. Purpose of This Study

This thesis is primarily focused on understanding the material characteristics and failure modes of Nicalon/CAS II in off-axis tensile loads. Specifically, this thesis involves: (1) observations of when and how damage initiates and progresses in off-axis tensile loads; (2) explain why they fail in the observed manner; and (3) compare the present test results with the available theories commonly used with polymeric composites.

C. Approach

Nicalon/CAS II fiber reinforced ceramic composite specimens, fabricated by Corning Glass Works Inc, were tested under off-axis tension to analyze damage initiation and progression and to relate off-axis strength and material properties test data with the present theories. The experiments were conducted at the USAF Material Laboratory, Wright-Patterson Air Force Base, Ohio. The composite tested

was an 8-ply, unidirectional laminate, with calcium aluminosilicate matrix, and continuous silicon carbide fiber. The panel was 153 mm by 153 mm (6 inches by 6 inches). The specimens were cut in six different orientations; 0, 15, 30, 45, 60, and 90 degrees off-axis. At least three specimens were made for each orientation. The specimens were polished on one edge in order to take micrographs of the material. Tensile tests were conducted at room temperature using a MTS test machine. The load was applied at 0.2 mm per minute. Acoustic Emission was used during testing to detect when the cracking started, and then replication of the edge was taken to confirm matrix cracking. A series of replications of a specimen at different load levels till its failure were taken to record damage progression. Mechanical properties were measured for both the longitudinal and transverse direction using strain gages mounted on one face in the load direction and 90 degrees from the load direction. Finally, the results were compared to present off-axis composite material theories for ultimate stress, modulus of elasticity and Poisson's ratio.

Chapter II will discuss previous related experimental investigations with ceramic composites of this type and the theoretical models commonly used to predict composites mechanical and material behaviors. Chapter III will give a description of the experimental procedure used for the testing of the composite. Chapter IV will present

discussion and results of the test and comparison of the test results to the theoretical models. Finally, Chapters V and VI will present conclusions and recommendations from this study respectively.

II. Background

Fiber reinforced ceramic composites are commonly referred to as brittle matrix composites (BMC). The main feature of BMCs are stiff matrices compared to the fiber and low strain to failure. Because of the low strain to failure of the matrix, matrix damage is usually present before final failure of the composite (4).

In this chapter previous related experimental works in crack initiation and progression, and crack density will be discussed. Also presented are related theoretical models for composite strength, material behaviors, and crack density.

A. Experimental Background

This section will give an overview of related experimental works in crack initiation and progression.

Recently Nicalon/CAS II has been investigated in several studies. Kim and Pagano (1) looked at initiation of damage in unidirectional Nicalon/CAS II under tensile loading. They found matrix cracking starts in the linear portion of the stress-strain curve. Daniel, Anastassopoulos and Lee (2), saw the same phenomenon.

Daniel et al also showed the composite would continue to develop matrix cracks until a certain crack density is reached, then the fibers would begin to fail. They also

showed the matrix-fiber interface does have some bonding properties where some ceramic composites such as SiC/LAS (3) show no bonding properties in the matrix-fiber interface and friction is the main method of transfer of load from matrix to fiber.

Kim and Katz (4) found a strain reversal in the transverse strain. This shows a relaxing of the matrix material in the transverse direction and the load is being carried by the fibers only in this region.

B. Theoretical Models

This section will present the theoretical models used is this thesis for predicting principal modulus of elasticity (E_1 and E_2), principal Poisson's ratio (ν_{12}), off-axis modulus of elasticity (E_x), off-axis Poisson's ratio (ν_{xy}), off-axis ultimate stress (σ_x^{ult}), and crack density. The principal direction elastic constants have been calculated assuming perfect bonding exists between the the fiber and the matrix which can be modified to assume no bonding. The off-axis elastic constants and ultimate stress can be predicted assuming an orthotropic material in plane stress using several methods. The crack density can be predicted for both strong and weak bonding of matrix and fiber.

1. Principal Material Properties.

The elastic modulus, E_1, along the fiber direction for

a well bonded composite can be estimated using the rule of mixtures (5:91):

$$E_1 = E_f V_f + E_m V_m \qquad (1)$$

where the subscript f denotes the fiber and m denotes the matrix. E is the elastic modulus and V is the volume fraction.

The transverse modulus, E_2, out of the four elastic constants, is the most difficult to calculate. E_2 can be predicted, for a well bonded composite, using the Halpin-Tsai equation (6):

$$E_2 = \frac{E_{2m}(1 + \zeta\eta V_f)}{(1 - \eta V_f)} \qquad (2)$$

where

$$\eta = \frac{\left[\frac{E_{2f}}{E_{2m}} - 1\right]}{\left[\frac{E_{2f}}{E_{2m}} + \zeta\right]} \qquad (3)$$

where

E_{2f} - transverse modulus of fiber

E_{2m} - transverse modulus of matrix

ζ - fiber packing geometry factor (ζ=2 for square packing)

Assuming their is a weak bond between the fibers and the matrix and the fibers do not contribute to the modulus

(E_{2f} = 0.0) then the Halpin-Tsai equation become (7:28):

$$E_2 = \frac{2E_{2m}(1 - V_f)}{(2 + V_f)} \qquad (4)$$

Bhatt and Phillips (7) showed the above modified Halpin-Tsai equation (eq 4) may give a good prediction for a weakly bonded BMC.

Poisson's ratio for unidirectional composites can be predicted by using the rule of mixtures:

$$\nu_{12} = \nu_{12f}V_f + \nu_{12m}V_m \qquad (5)$$

where the subscript f and m refer to fiber and matrix respectively.

There are relationships for G_{12} for strong bonded composites which were modified by Bhatt et al (7) for weak bonded composites. This paper will not discuss G_{12} because G_{12} was not obtained experimentally due to limited material.

2. Off-axis Material Properties Theoretical Models.

The off-axis material properties are formulated here as outlined in Jones (5:48-56). Transformation of stress and strain from the 1-2 coordinate system to the x-y coordinate system (Figure 1) is accomplished as follows:

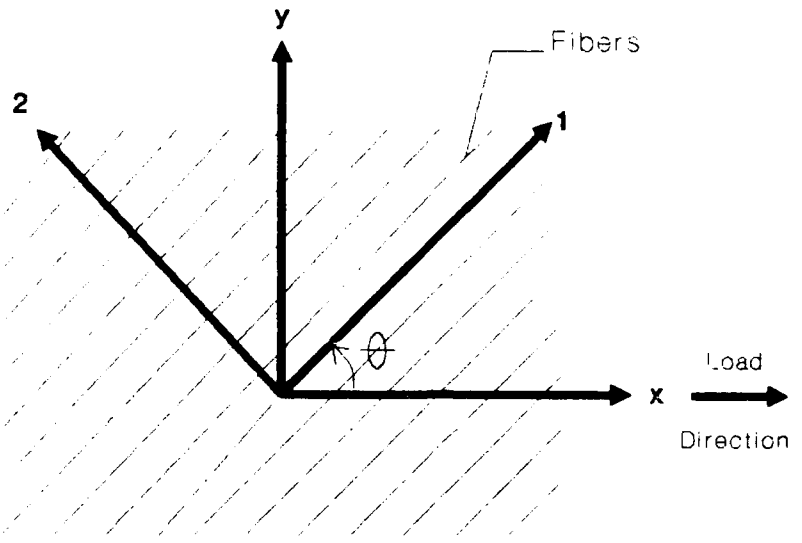

Figure 1 Rotation of Principlie Material Axis to Arbitrary x-y Axis

$$\begin{Bmatrix} \sigma_x \\ \sigma_y \\ \tau_{xy} \end{Bmatrix} = [T]^{-1} \begin{Bmatrix} \sigma_1 \\ \sigma_2 \\ \tau_{12} \end{Bmatrix} \tag{6}$$

$$\begin{Bmatrix} \varepsilon_x \\ \varepsilon_y \\ \gamma_{xy} \end{Bmatrix} = [R][T]^{-1}[R]^{-1} \begin{Bmatrix} \varepsilon_1 \\ \varepsilon_2 \\ \gamma_{12} \end{Bmatrix} \tag{7}$$

where

$$[T] = \begin{bmatrix} \cos^2\theta & \sin^2\theta & -2\sin\theta\cos\theta \\ \sin^2\theta & \cos^2\theta & 2\sin\theta\cos\theta \\ \sin\theta\cos\theta & -\sin\theta\cos\theta & \cos^2\theta - \sin^2\theta \end{bmatrix} \tag{8}$$

$$[R] = \begin{bmatrix} 1 & 0 & 0 \\ 0 & 1 & 0 \\ 0 & 0 & 2 \end{bmatrix} \tag{9}$$

The stress-strain relationship for an orthotropic material in plane stress is:

$$\begin{Bmatrix} \varepsilon_1 \\ \varepsilon_2 \\ \tau_{12} \end{Bmatrix} = \begin{bmatrix} S_{11} & S_{12} & 0 \\ S_{12} & S_{22} & 0 \\ 0 & 0 & S_{66} \end{bmatrix} \begin{Bmatrix} \sigma_1 \\ \sigma_2 \\ \tau_{12} \end{Bmatrix} \tag{10}$$

Substituting into eqn (10) eqn (6) and (7) gives:

$$\begin{Bmatrix} \varepsilon_x \\ \varepsilon_y \\ \gamma_{xy} \end{Bmatrix} = [R][T]^{-1}[R]^{-1}[S][T] \begin{Bmatrix} \sigma_x \\ \sigma_y \\ \tau_{12} \end{Bmatrix} = \begin{bmatrix} \bar{S}_{11} & \bar{S}_{12} & \bar{S}_{16} \\ \bar{S}_{12} & \bar{S}_{22} & \bar{S}_{26} \\ \bar{S}_{16} & \bar{S}_{26} & \bar{S}_{66} \end{bmatrix} \begin{Bmatrix} \sigma_x \\ \sigma_y \\ \tau_{12} \end{Bmatrix} \tag{11}$$

where,

$$[\bar{S}] = [R][T]^{-1}[R]^{-1}[S][T] \tag{12}$$

and,

$$\begin{aligned}
\bar{S}_{11} &= S_{11}\cos^4\theta + (2S_{12} + S_{66})\sin^2\theta\cos^2\theta + S_{22}\sin^4\theta \\
\bar{S}_{12} &= S_{12}(\sin^4\theta + \cos^4\theta) + (S_{11} + S_{22} - S_{66})\sin^2\theta\cos^2\theta \\
\bar{S}_{22} &= S_{11}\sin^4\theta + (2S_{12} + S_{66})\sin^2\theta\cos^2\theta + S_{22}\cos^4\theta \\
\bar{S}_{16} &= (2S_{11} - 2S_{12} - S_{66})\sin\theta\cos^3\theta - (2S_{22} - 2S_{12} - S_{66})\sin^3\theta\cos\theta \\
\bar{S}_{26} &= (2S_{11} - 2S_{12} - S_{66})\sin^3\theta\cos\theta - (2S_{22} - 2S_{12} - S_{66})\sin\theta\cos^3\theta
\end{aligned} \tag{13}$$

$$\bar{S}_{66} = 2(2S_{11} + 2S_{22} - 4S_{12} - S_{66})\sin^2\theta\cos^2\theta + S_{66}(\sin^4\theta + \cos^4\theta) \quad \text{(13 cont)}$$

for an orthotropic material:

$$S_{11} = \frac{1}{E_1}$$

$$S_{12} = -\frac{\nu_{12}}{E_1} \quad (14)$$

$$S_{22} = \frac{1}{E_2}$$

$$S_{66} = \frac{1}{G_{12}}$$

Substituting equations (14) into equations (13) and then substituting x, y, and $\bar{S}_{ij}$ for 1, 2, and S respectively in equations (14) and substituting these into equations (13) also, the following equations are obtained:

$$\frac{1}{E_x} = \frac{1}{E_1}\cos^4\theta + \left(\frac{1}{G_{12}} - \frac{2\nu_{12}}{E_1}\right)\sin^2\theta\cos^2\theta + \frac{1}{E_2}\sin^4\theta \quad (15)$$

$$\nu_{xy} = E_x\left[\frac{\nu_{12}}{E_1}(\sin^4\theta + \cos^4\theta) - \left(\frac{1}{E_1} + \frac{1}{E_2} - \frac{1}{G_{12}}\right)\sin^2\theta\cos^2\theta\right] \quad (16)$$

$$\frac{1}{E_y} = \frac{1}{E_1}\sin^4\theta + \left(\frac{1}{G_{12}} - \frac{2\nu_{12}}{E_1}\right)\sin^2\theta\cos^2\theta + \frac{1}{E_2}\cos^4\theta \quad (17)$$

$$\frac{1}{G_{xy}} = 2\left(\frac{2}{E_1} + \frac{2}{E_2} + \frac{4\nu_{12}}{E_1} - \frac{1}{G_{12}}\right)\sin^2\theta\cos^2\theta + \frac{1}{G_{12}}(\sin^4\theta + \cos^4\theta) \quad (18)$$

In this paper only the equations for E_x and ν_{xy} will be used because test data for G_{xy} was not obtained.

3. Ultimate Strength Theoretical Model.

There are several failure criteria models for off-axis loading. This section will outline the Tsai-Hill failure criterion.

The off-axis ultimate strength of the composite can be predicted knowing the axial and transverse ultimate strength in the principal directions by using the Tsai-Hill failure criterion. Hill (8) proposed a failure criterion for anisotropic material:

$$(G+H)\sigma_1^2+(F+H)\sigma_2^2+(F+G)\sigma_3^2-2H\sigma_1\sigma_2-2G\sigma_1\sigma_3-2F\sigma_2\sigma_3+2L\tau_{23}^2 +2M\tau_{13}^2+2N\tau_{12}^2 = 0 \quad (19)$$

The strengths F, G, H, L, M, and N can be regarded as failure strengths. Tsai (9:3-11) related F, G, H, L, M, and N to the usual failure strengths X, Y, and S for a lamina. If each applied load is taken as the only load, τ_{12}, σ_1, $\sigma_2$and σ_3 and make it equal to the maximum load S, X, Y and Z respectively you get:

for $\tau_{12} \neq 0$ $$2N = \frac{1}{S^2} \quad (20)$$

for $\sigma_1 \neq 0$ $$G + H = \frac{1}{X^2} \quad (21)$$

for $\sigma_2 \neq 0$ $$F + H = \frac{1}{Y^2} \quad (22)$$

for $\sigma_3 \neq 0$ $$F + G = \frac{1}{Z^2} \quad (23)$$

Solving for F, G, and H in terms of X, Y, and Z you get:

$$2H = \frac{1}{X^2} + \frac{1}{Y^2} - \frac{1}{Z^2} \quad (24)$$

$$2G = \frac{1}{X^2} - \frac{1}{Y^2} + \frac{1}{Z^2} \quad (25)$$

$$2F = -\frac{1}{X^2} + \frac{1}{Y^2} + \frac{1}{Z^2} \quad (26)$$

For plane stress in the 1-2 plane σ_3, τ_{13}, and τ_{23} are zero. The 1 direction is the direction of the fibers. Because of symmetry in the 2 and 3 directions Z = Y. Putting these assumptions and eqns (24), (25), and (26) into eqn (19) the following is obtained:

$$\frac{\sigma_1^2}{X^2} - \frac{\sigma_1\sigma_2}{X^2} + \frac{\sigma_2^2}{Y^2} + \frac{\tau_{12}^2}{S^2} = 1 \quad (27)$$

Finally, for an off-axis stress, substitute the transformation equations for a uniaxial stress:

$$\sigma_1 = \sigma_x \cos^2\theta \quad (28)$$

$$\sigma_2 = \sigma_x \sin^2\theta \quad (29)$$

$$\tau_{12} = -\sigma_x \sin\theta \cos\theta \quad (30)$$

into eqn (27) to get the Tsai-Hill failure criteria:

$$\frac{\cos^4\theta}{X^2} + \left[\frac{1}{S^2} - \frac{1}{X^2}\right] \cos^2\theta \sin^2\theta + \frac{\sin^4\theta}{Y^2} = \frac{1}{\sigma_x^2} \quad (31)$$

This is not the most general theory such as the Tsai-Wu (10)

but because of the limited information about the ceramic composites strengths, the Tsai-Hill is the easiest to use.

4. Crack Density Theoretical Models.

The information on matrix cracking has been used to understand what is happening at the matrix-fiber interface. This section will outline a theoretical model proposed by Aveston, Kelly, and Cooper (11) and Aveston and Kelly (12) for a weak bond between the matrix and fiber and a strong bond respectively.

Aveston, Kelly, and Cooper (11) studied matrix cracking behavior in unidirectional composites under tension loading (parallel to the fibers). In composites, where the breaking strain of the fiber is much greater than in the matrix, after initial matrix cracking starts, the fibers will prevent the matrix from opening up further. As the stress is increased, the matrix will crack in another area. There are two limiting cases after the first matrix cracking appears; (1) unbonded case where there is no elastic bonding between the fiber and the matrix and (2) the bonded case where there is a linear elastic bonding between the fiber and matrix after the matrix cracking takes place.

In the first case Aveston, Cooper, and Kelly (11) said once a limiting shear stress (τ') was exceeded the fibers can move through the matrix. For this unbonded case τ' is a constant. And according to Aveston et al, matrix cracking will occur with a spacing between x' and 2x' where:

$$x' = \frac{V_m \sigma_{1m}^{ult} r}{V_f 2\tau'} \qquad (32)$$

where,

r - radius of the fiber

σ_{im}^{ult} - ultimate stress of the matrix

Further increase in strain after the cracking is complete is absorbed by the fiber only and Young's modulus of the material becomes $E_f V_f$.

For the second case, with linear elastic bond between the fiber and matrix, Aveston and Kelly (12) proposed that after the first crack has occurred in the matrix the additional stress placed on the fiber has a maximum value of $\Delta\sigma_o$ at the plane of the matrix crack and becomes less farther away from the crack. According to Aveston and Kelly (12) the minimum spacing between cracks transverse to a zero degree specimen is between δ and 2δ, where:

$$\delta = -\frac{1}{\phi \cdot 5} \log \left[1 - \frac{\sigma_{1m}^{ult} V_m}{\Delta\sigma_o V_f} \right] \qquad (33)$$

where,

σ_{1m}^{ult} - Tensile strength of matrix

V_f - fiber volume ratio

V_m - matrix volume ratio

$\Delta\sigma_o$ - incremental stress carried by the fibers after matrix cracking

$$\Delta\sigma_o = \frac{\sigma}{V_f} - \varepsilon_{1m}^{ult} E_{1f} \tag{34}$$

where,

σ - applied stress

ε_{1m}^{ult} - ultimate tensile strain of matrix

E_{1f} - fiber modulus

$$\phi = \left[\frac{2G_{12m}E_1}{E_{1f}E_{1m}V_f}\right] \frac{1}{r^2 \log(R/r)} \tag{35}$$

where,

E_{1m} - matrix modulus

E_1 - composite modulus

G_{12m} - matrix shear modulus

r - fiber radius

2R - center to center distance between fibers

These theories can be used to show if there is any bonding between the fiber and matrix, according to Daniel et al (2).

III. Experimental Procedure

This chapter will discuss sample preparation, test procedures, and data reduction.

A. Sample Preparation

This section will describe the material, discuss how the fiber volume fraction was obtained, and how the specimens were prepared.

The material, Nicalon/CASII (serial #8834301L), was obtained from Corning Glass Works in December 1988. The material was fabricated in a 153 mm square plate, eight plys thick, and unidirectional fibers. The fibers are continuous silicon carbide. The matrix is a calcium aluminosilicate ceramic material developed by Corning Glass Works. From Daniels et al (2), the properties of the matrix, fiber and composite from various tests are tabulated in Table 1. The plate was dark, almost black, on one side and light gray on the other. The light gray side had a thicker coating of matrix than the dark side.

The volume fiber fraction (V_f) was obtained by taking sixteen micrographs of the 90° specimen at 100x, see Figure 2. Figure 2 shows some voids that were inherent in the material. The figure also shows that the fibers have different diameters and uneven distribution. An

Table 1
Matrix, Fiber and Composite Material Properties

Property	Matrix (CASII)	Fiber (Nicalon)	Nicalon/ CASII
Ultimate Axial Stress (σ_1^{ult}) MPa	124	2060	266
Ultimate Transverse Stress (σ_2^{ult}) MPa	same as above	same as above	21
Ultimate Shear Stress (S) MPa	-	-	38(+)
Axial Modulus (E_1) GPa	200(**)	98(*)	139
Transverse Modulus (E_2) GPa	200	98	97
Shear Modulus (G_{12}) GPa	96(+)	167(***)	44(++)
Poissons Ratio (ν_{12})	-	-	.247
Fiber Volume (V_f)	-	-	.34(+++)

(*) Obtained from references (14) and (15)
(**) Obtained from reference (2)
(***) Obtained from reference (7)
(+) Corning Glass Works Material specification sheet
(++) Using 15 degree data and equation (15) for off-axis material properties
(+++) Obtained from volume fraction study outlined in this chapter

all other data from test results

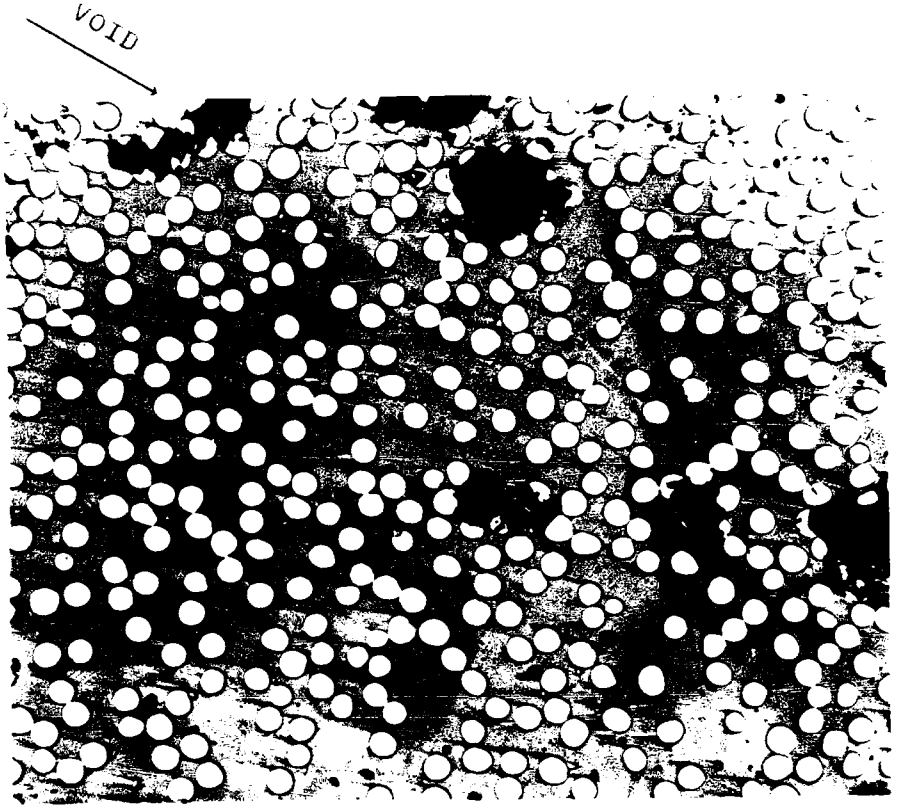

Figure 2 Volume Fraction Calculations Picture (100x)

average fiber cross-section area was calculated measuring 50 fibers with a 1/100th inch ruler. The number of fibers were counted in each micrograph and V_f was calculated using the following formula:

$$V_f = \frac{nA_f}{A_p} \qquad (36)$$

where,

n - number of fibers

A_f- cross section of the fibers

A_p- cross section of the picture

Then the sixteen V_f's were averaged to give a composite fiber volume fraction, which was found to be 0.34.

The material was cut using a Buehler Isomet Low Speed Saw with a diamond blade. The plate was cut in six off-axis orientations. One large piece for each orientation was cut as shown in Figure 3, then three specimens were cut from this large piece, as shown by the dotted lines. The nominal width of all the specimens was approximately 7.6 mm. Table 3 in the appendix gives each specimens width, thickness, and gage length. The orientations were cut in the following order to reduce the amount of waste and to simplify the cutting; 0°, 90°, 15°, 45°, 30°, and finally the 60°. Later it was necessary to cut additional 45, 60, and 90 degree specimens from the rest of the plate as shown by the thinner

specimens in Figure 3.

After cutting, as described above, beveled end tabs were attached to the ends of the specimens for gripping during testing. The tabs were made of $0/90^{\circ}$ fiberglass epoxy. The tabs were bonded using epoxy cement cured at $200^{\circ}F$ for 2 hours. The tabs were of different lengths and placed on the specimens giving different gage lengths depending on the orientation of the fibers. The 60° and 90° specimens did not have tabs because a different gripping technique was employed as discussed later. The usual specimen lengths and configurations for the different fiber orientations are shown in Figure 4.

After tabbing the specimens were polished on one of its edges, see Figure 5 for terminology, to enhance microscopic imaging and replication for crack detection. A polishing fixture, as shown in Figure 6, was used to polish two specimens at a time. First, the specimens were polished on a flat surface with aluminum oxide sand paper using successively smaller grit sizes (120, 240, 300, 420, and 600 grit). Then, on a polishing wheel with 3 micron alumina and finally, on the polishing wheel with .05 micron alumina.

Next two 350Ω strain gages (Micro Measurements Type CEA-06-2UW-350) were attached to one side of each specimen, one in the axial load direction and one in the transverse, see Figure 5.

Each specimen's thickness and width were measured using

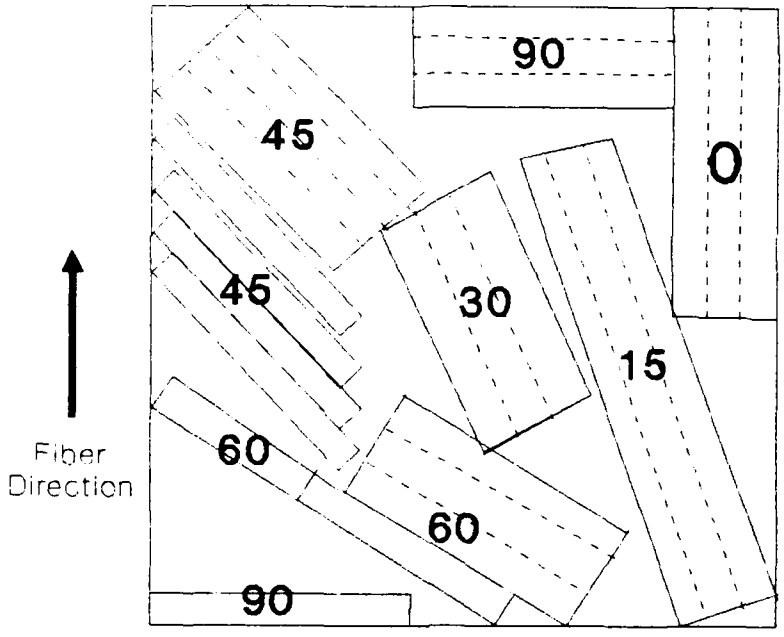

Figure 3 Off-axis Cut Out of 152 mm Square Panel

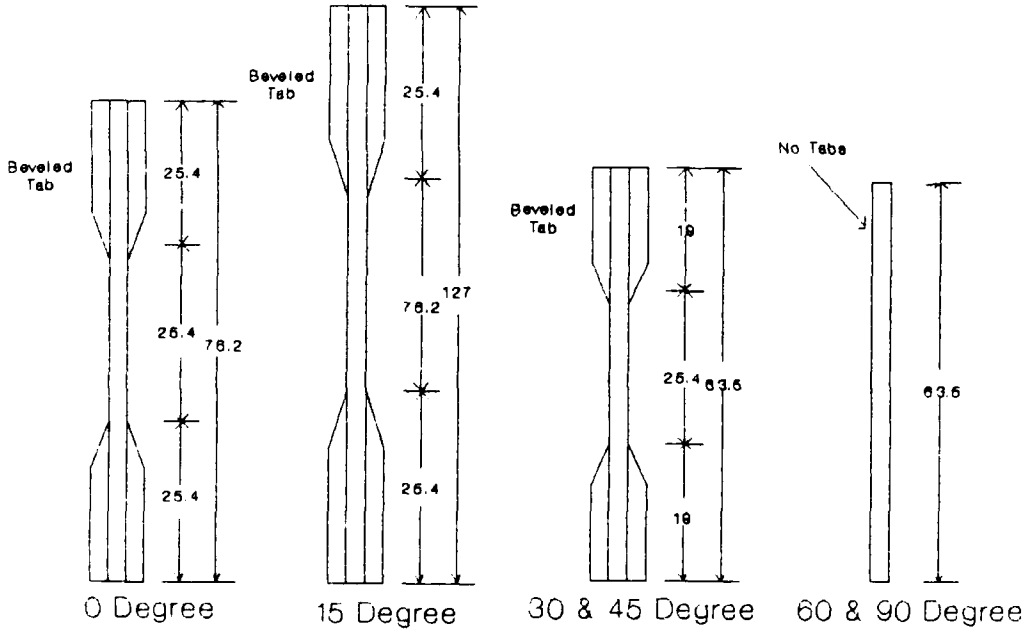

Figure 4 Typical Specimen Dimensions (mm)

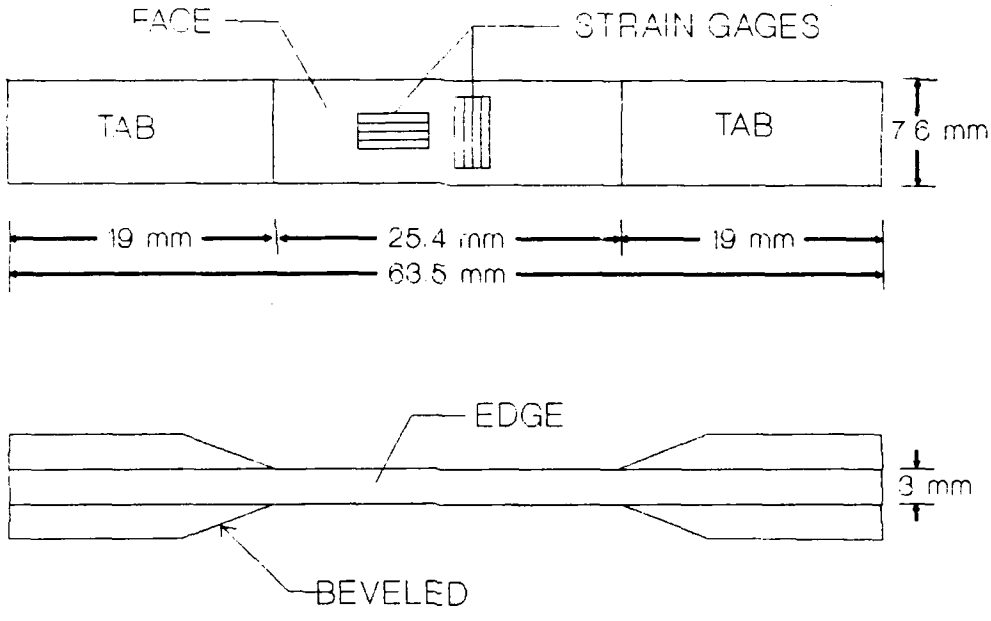

Figure 5 General Specimen Layout

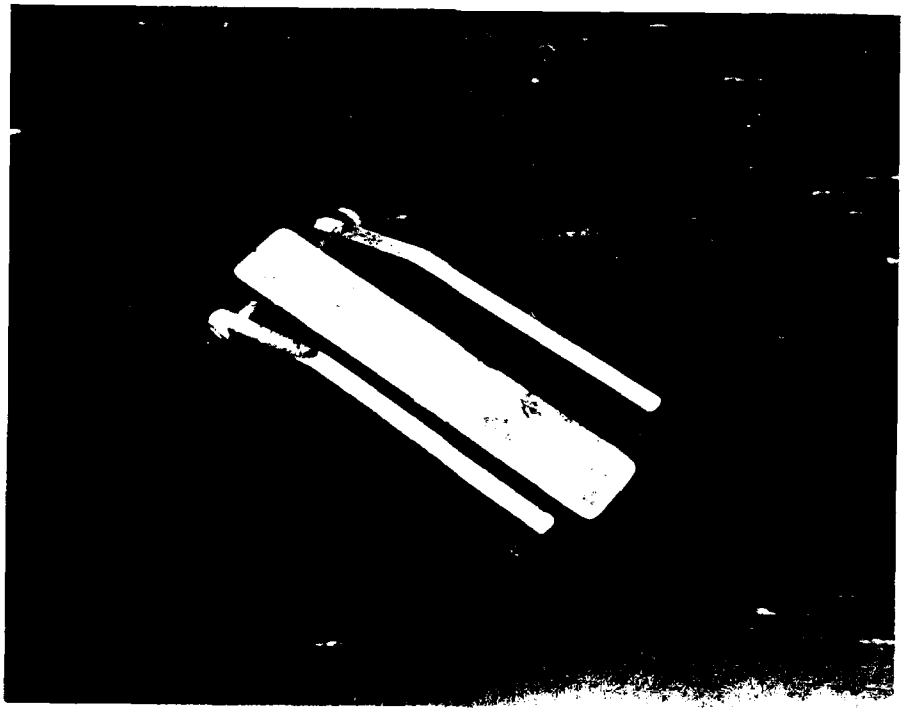

Figure 6 Polishing Fixture

a micrometer to determine the cross-sectional area.

B. Test Procedures

This section will discuss the test procedures, replication, and acoustic emission. The specimens were mounted on a MTS load frame (Figure 7), with acoustic emission attached to the specimen face. The 60^{o} and 90^{o} specimens were mounted in the MTS frame in a fixture, as shown in Figure 8. The fixture was first loaded in the frame without the specimen in it, then the specimen was glued into the fixture with Hardman Epoweld 8173 5-minute epoxy adhesive. This was done because the 60 and 90 degree specimens were breaking when the specimen was being put in the MTS grips. This probably was caused by bending of the specimen due to grip alignment limitations of the MTS load frame. The specimens with other off-axis load orientations were loaded directly into the MTS frame with a 500 psi grip load. Acoustic emission was used to detect when the initial cracking occurred. The acoustic emission was set with a threshold of 40 db.

One specimen of each orientation was loaded in tension at a cross head speed of 0.2 mm/minute until final failure annotating when the acoustic emission first began to detect noise in the specimen. To obtain the material properties of each fiber orientation, the load and strain during the testing were monitored on an x-y plotter.

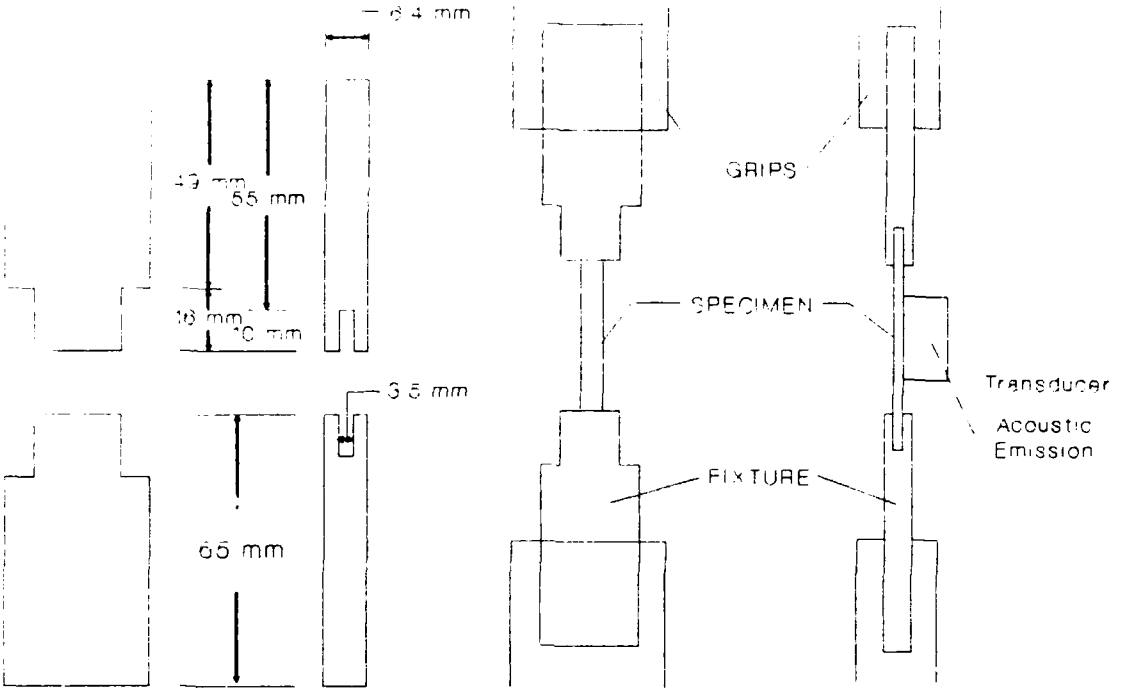

Figure 7 60 and 90 Degree Specimen Fixture Dimensions

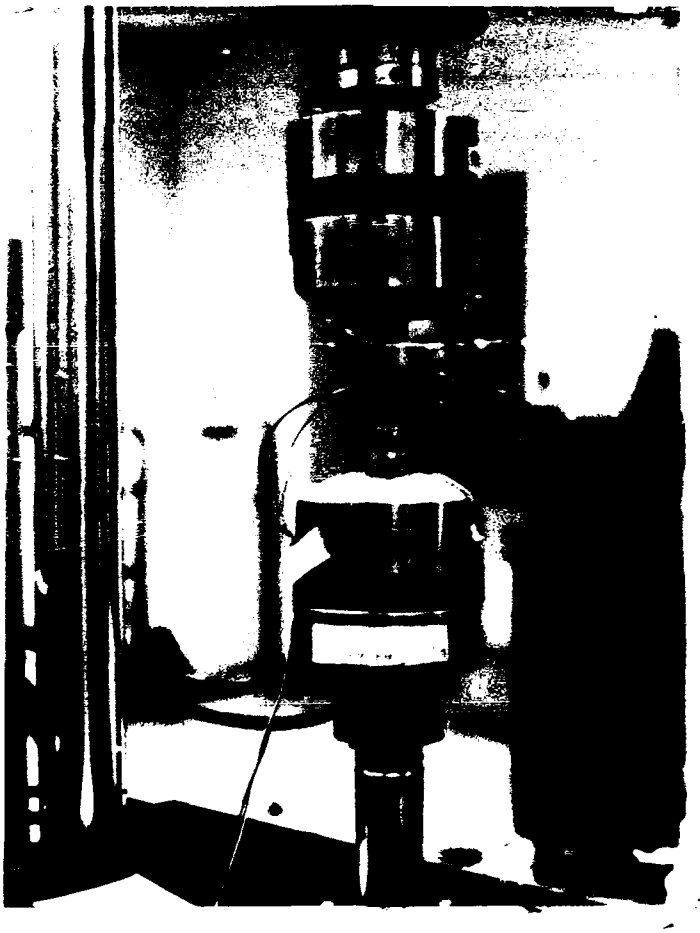

Figure 8 MTS Machine With Specimen Installed

The next specimen was loaded to a point right before the acoustic emission reading were seen in the previous test. The load was held and a replica was made of both the face and edge of the specimen to see if additional cracks had started. Then the load was taken down to zero and increased until an acoustic emission was detected. Another replication was taken to see if cracking of the specimen had started. This was done until a crack in the specimen was found. For the 0° and 15° specimens this procedure was repeated several times in order to evaluate the damage progression with increased stress and strain.

To observe and record the formation and progression of damage, micrographs were taken from the replications and fractured specimen using an Olympus inverted metallurgical microscope with a Polaroid camera as shown in Figure 9. The magnification power of the microscope ranged from 50x to 1000x, however only magnification of 200x was sufficient for the present work.

C. Data Reduction

The ultimate failure stress for each off-axis loading was calculated using the point of maximum load on the graph obtained by the x-y plotter monitoring the force and strain during testing. The modulus of elasticity, E_x, was calculated by taking the slope of the linear portion of the recorded stress-strain curve. Poisson's Ratio was

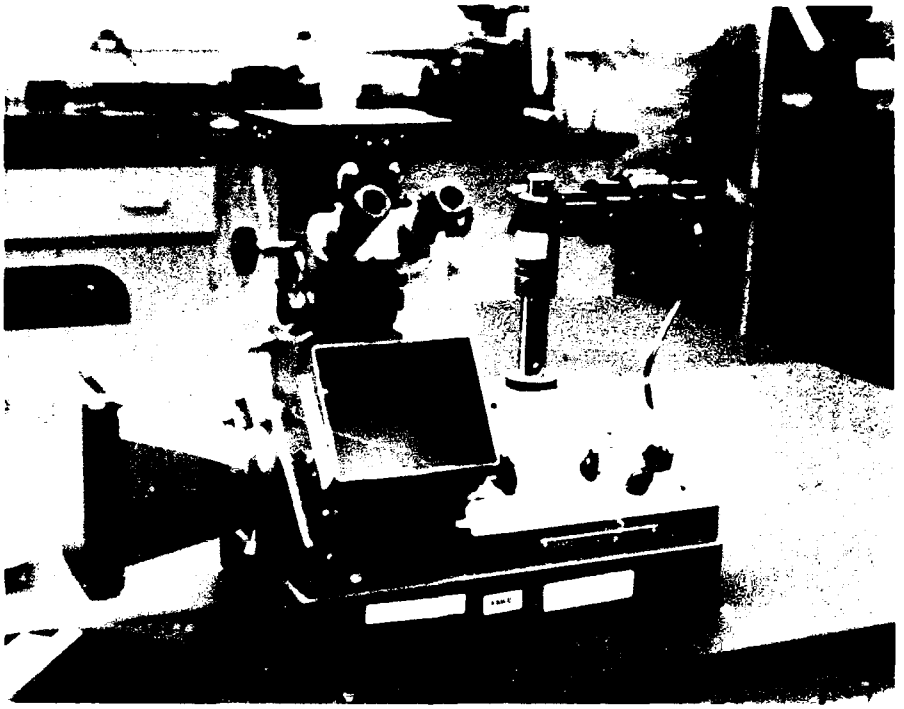

Figure 9 Microscope with Polaroid Camera

calculated using the slopes of the linear portion of both the axial and transverse stress-strain curves. Poisson's ratio was calculated by taking the ratio of the strain in the transverse direction and dividing it by the strain in the axial direction. The stress-strain curves presented in this thesis were made using the data from the x-y plotter and transferring points into a graphics program manually.

The crack density was obtained by counting the number of cracks in a micrograph of the specimen or replication. For the crack density where one or less cracks were in one picture, the crack density was averaged by counting all the cracks in a replication and dividing it by the length of the replication.

IV Results and Discussion

This chapter contains the results and discussion of the experimental tests and comparisons of the test data to the theoretical models. The first part of the chapter will discuss the general problems related to the tested ceramic composite material and specimen preparation. The next part will discuss the crack initiation and progression in each off-axis load orientation separately. And the final section will discuss the overall test results along with comparison of the test results to the existing theoretical models.

A. Material Preparation

Several problems with material preparation were encountered throughout testing of the ceramic composite. The panel was a light grey on one side and a dark grey to black on the other side. The light gray side had a thicker coating of matrix material than the black one. This coating had several hairline cracks in it. Most of the cracks were from the edge of the coating to the first layer of fibers. A few of these cracks extended into the first ply of the material but both cases behaved (during testing) in the same manner. Micrographs were taken for each of the hairline cracks for several specimens. Figure 10 shows an example of one hairline crack before the specimen was tested and after

(a) Before Loading (100x)

(b) After Loading (200x)

Figure 10 Hairline Crack in Matrix Before and After Loading Specimen 45-5

the specimen was loaded and failed. As can be seen in the pictures the hairline crack on the edge and in the middle of the picture did not grow after loading. Also, failure of the specimen did not occur at any of the micrographed hairline cracks before testing. Therefore, it is concluded that the hairline cracks did not effect the properties of the material.

The hairline cracks were probably caused by the polishing operation. There were some of these hairline cracks in the panel before cutting was started, but they were not dense enough to account for all the matrix cracking in the specimen, after preparation. These cracks on the edge could be noticed easily after polishing. The specimens were polished with the tabs already on. The polishing tool might have bent the specimen causing the cracks to form in the matrix.

One 60, one 45, and one 90 degree specimen each had large cracks all the way through the matrix. This was not noticed until after polishing. The cracks were probably in the material before polishing was started, but could not be seen until the polishing was completed. These specimens, with the cracks in the material, were not used. If there was enough material to use, the part of the specimen with the crack in it was cut off.

On the black side along the edges of the panel the material had large voids where bare fibers could be seen.

Figure 11 shows the void on the left side of the picture, with the horizontal fibers showing through. This was due to an inadequate amount of matrix applied along the edge of the panel during manufacturing. This effected only a small area at the edge of the panel. Only three specimens had gage lengths in these areas, and part of the bad areas were polished off. Also, the ultimate strengths of the specimens taken from this area showed no observable difference in strength from the other specimens.

B. Damage Initiation and Progression

This section discusses the damage initiation and damage progression for each load orientation separately. The crack initiation, crack progression and stress strain curve will be discussed.

First a specimen of each off-axis load orientation was tested to failure without stopping. Acoustic emission was used to monitor cracking noise. The remaining specimens for each load orientation were, thereafter, loaded to several different load levels. These specimens, in each off-axis orientation, were loaded to a stress level right before the acoustic emission detected noise on the first specimen, a replication was taken to verify matrix cracking had not started, then it was unloaded. It was then loaded until the acoustic emission detected a crack and a replication was taken of both the face and the edge to verify whether a

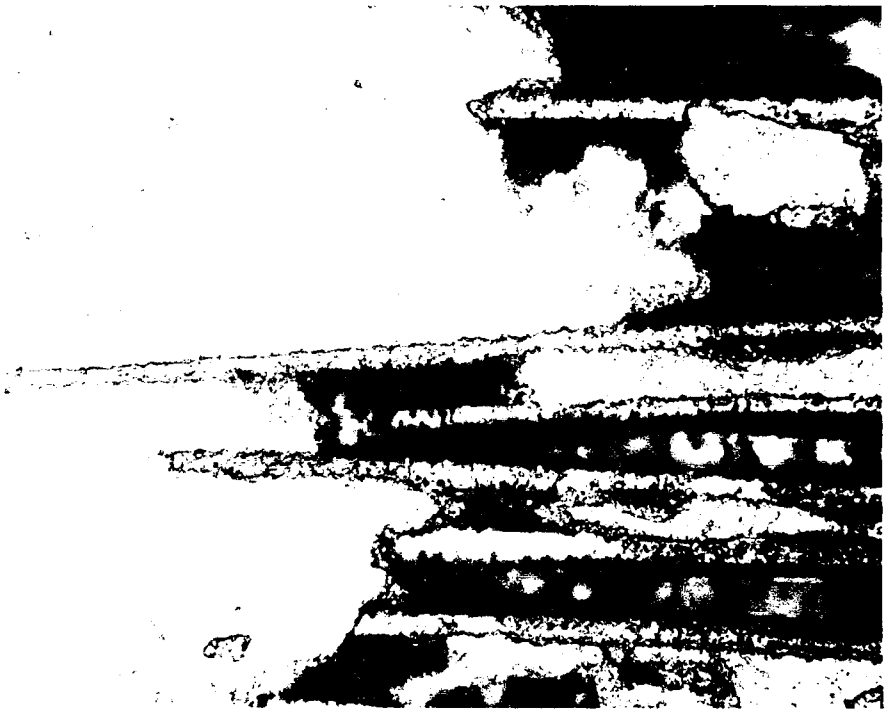

Figure 11 Voids on Surface of Panel Before Cutting (400x)

crack had started. This procedure was continued until a crack was found or the specimen failed.

Acoustic emission seemed to do a good job in determining when cracking started. The acoustic emission rarely had a false alarm and from the tests where the loading was stopped before an emission was detected no cracking was missed by this method.

The overall test results are shown in Table 2. This table shows the results for each specimen and the average for each load orientation. Tabulated are the modulus of elasticity, ultimate stress and strain, and matrix cracking stress and strains. The subscript x and y denotes the direction of the load and the direction perpendicular to the load respectively. The superscript "ult" denotes the ultimate value (where total failure took place) and the "mc" denotes when matrix cracking was first observed. Most failures occurred in the gage length, exceptions are annotated in Table 2 in the notes column.

1. 0-degree Specimen

This load orientation will be analyzed more thoroughly than the others. Observations of crack initiation and progression will be discussed. Also several features of the stress-stain curve are discussed.

During the testing of the 0^{o} specimen, replication and acoustic observations showed that the matrix cracking started during the linear portion of the stress-strain

Table 2 Summary of Test Results

Specimen Number	E_x (GPa)	ν_{xy}	σ_x^{ult} (MPa)	ε_x^{ult} ($\mu\varepsilon$)	ε_y^{ult} ($\mu\varepsilon$)	σ_x^{mc} (MPa)	ε_x^{mc} ($\mu\varepsilon$)	ε_y^{mc} ($\mu\varepsilon$)	Notes
0-1	142.0	.264	281.7	3315	-480	82.6	600	-150	
0-2	140.7	.23	254.0	3360	-150	94.9	675	-120	
0-3	134.9	.248	262.2	3750	-255	70.4	500	-131	
Avg	139.2	.247	265.9	3475	-295	82.5	592	-134	
15-1	130.4	.25	121.8	900	-252	49.7	450	-114	
15-2	139.3	.248	128.7	995	-252	90.0	645	-177	
15-3	138.9	.24	119.9	800	-180	70.1	495	-125	
Avg	136.2	.246	125.2	899	-228	69.9	530	-139	
30-1	120.0	.23	64.5	522	-142	*	*	*	
30-2	123.0	.223	79.7	630	-170	*	*	*	
30-3	124.4	-	-	-	-	-	-	-	(1)
Avg	122.4	.227	72.1	576	-156	*	*	*	
45-1	-	-	-	-	-	-	-	-	(2)
45-2	-	-	-	-	-	-	-	-	
45-3	124.1	.22	-	-	-	-	-	-	(1)
45-4	115.6	.225	-	-	-	-	-	-	(1)
45-5	116.2	.24	49.1	590	-98	40.2+	320+	-80+	(3)
45-6	-	-	-	-	-	-	-	-	(1)
45-7	110.2	.20	51.0	552	-87	33.1+	240+	-75+	
45-8	118.4	.195	42.7	357	-99	42.7	357	-99	
Avg	116.9	.216	47.6	500	-94	38.7	306	-85	
60-1	116.8	.20	24.5	210	-45	*	*	*	
60-2	128.3	.239	34.9	-	-72	*	*	*	(3)
60-3	-	-	-	-	-	-	-	-	(2)
60-4	109.6	.194	23.1	270	-51	*	*	*	(3)
60-5	93.9	.174	23.9	260	-58	*	*	*	
Avg	112.2	.202	26.6	247	-56	*	*	*	
90-1	79.1	-	21.2	258	-	*	*	*	
90-2	102.1	-	-	-	-	-	-	-	(1)
90-3	108.9	-	20.7	188	-	*	*	*	(3)
90-4	81.1	.164	15.3	206	-33	*	*	*	
Avg	92.8	.164	19.1	217	-33	*	*	*	

mc - Matrix cracking starts
+ - Assumes cracking starts at nonlinear part of stres-strain curve
* - Matrix cracking strain is the same as the ultimate strain
(1) - Broke due to bad alignment of grips
(2) - Cracked before loading
(3) - Broke in tab area

curve. Ultimate failure occurred within the gage length of the specimen. The average values for the ultimate stress and strain are 266 MPa and 3475 $\mu\varepsilon$ respectively. Matrix cracking was observed to start at an average value of 83 MPa and 590 $\mu\varepsilon$. This stress level is 30 percent of the ultimate stress of 266 MPa. Figure 12 is a computer generated graph of a typical stress-strain curve and acoustic emission output. Notice that the matrix cracking begins where the acoustic emission starts to detect noise and it starts in the linear portion of the stress-strain curve.

The initial cracking was randomly distributed at first, then became continuous across the edge with increase in load. Figures 13a-e shows how crack spacing changes from loads of 115 MPa to 250 MPa. These pictures were taken at the same spot on the specimen. Figure 13a shows an initial crack in the right hand corner when the stress was 115 MPa. Figure 13b shows two small cracks in the right hand corner when the stress was 160 MPa. Then the cracking becomes more continuous through the edge and crack spacing is more even, as seen in Figure 13c at 218 MPa. Figure 13d shows the crack spacing decreases further at 250 MPa. Finally, at failure Figure 13e shows the crack spacing is the same as seen in the previous picture. The matrix crack density will be further discussed in a later section of this chapter. Since the matrix cracking begins in the linear portion

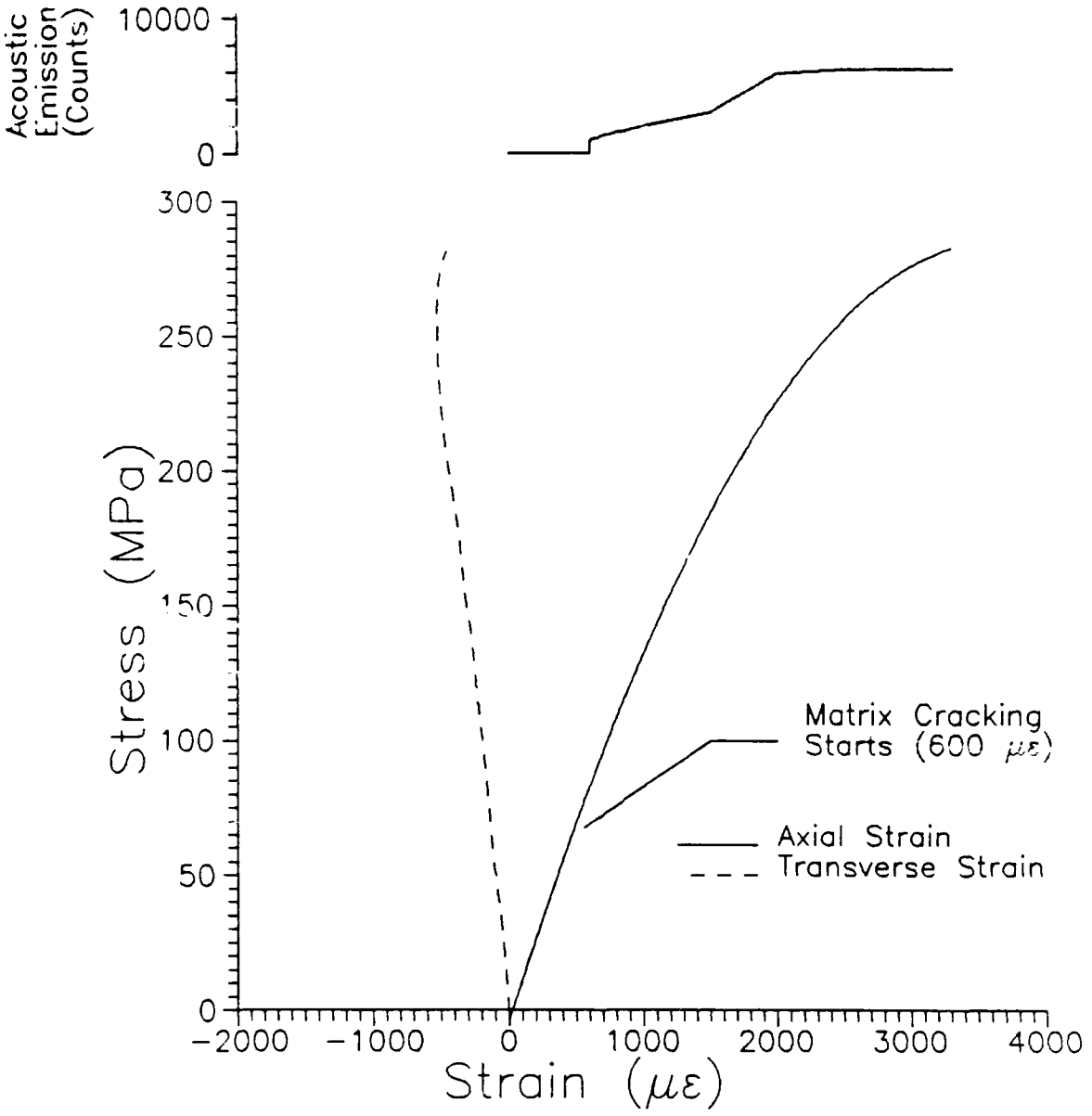

Figure 12 Stress vs Strain and Acoustic Emission for 0 Degree Specimen (0-1)

(a) Edge at 115 MPa (100x)

(b) Edge at 159 MPa (100x)

Figure 13 Crack Progression for 0 Degree Specimen (115-250 MPa) Specimen 0-2

(c) Edge at 218 MPa (100x)

(d) Edge at 250 MPa (100x)

Figure 13 (cont)

(e) Edge at 254 MPa (Failure) (200x)

Figure 13 (cont)

of the stress-strain curve, the beginning of failure is not indicated by the nonlinearity of the stress-strain curve. This has been seen by Kim and Pagano (1) and Daniel et al (2) in this material and other similar materials.

Both the axial and transverse stress-strain curves have a nonlinear portion before failure. Figure 12 shows the axial stress-strain curve which is of the same shape as any common material, it has a linear portion and gently curves before failure. The transverse strain , on the other hand, is actually reversing its direction before final failure. Figure 14 shows a typical transverse strain response seen during this test, it is expanded to clarify this feature. It seems that when the transverse strain reverses direction, the matrix has cracked as much as it can and the fiber is beginning to carry all the load. Physically the matrix has quit compressing in the transverse direction and the matrix has begun to relax back. The fibers are probably beginning to debond from the matrix at this point. This phenomena was first observed by Kim and Katz (4).

Also observed during the incremental loading was a change in the modulus of elasticity. Figure 15 shows the response of this material under the loading and unloading procedures. The first set of tests consisted of loading up in the linear range (ie to pt A), in the second set of tests it was loaded to just past pt A (into the nonlinear range),

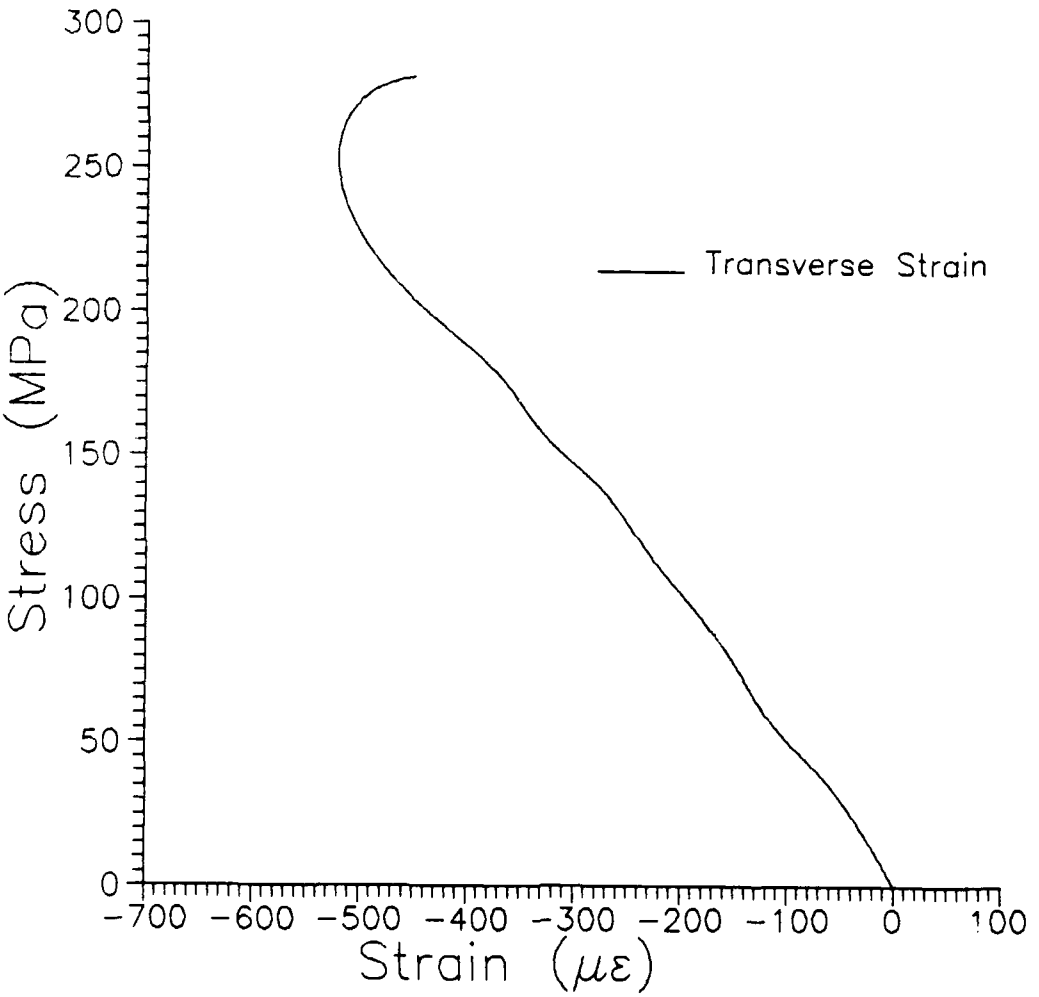

Figure 14 Transverse Stress vs Strain for 0 Degree Specimen (0-2)

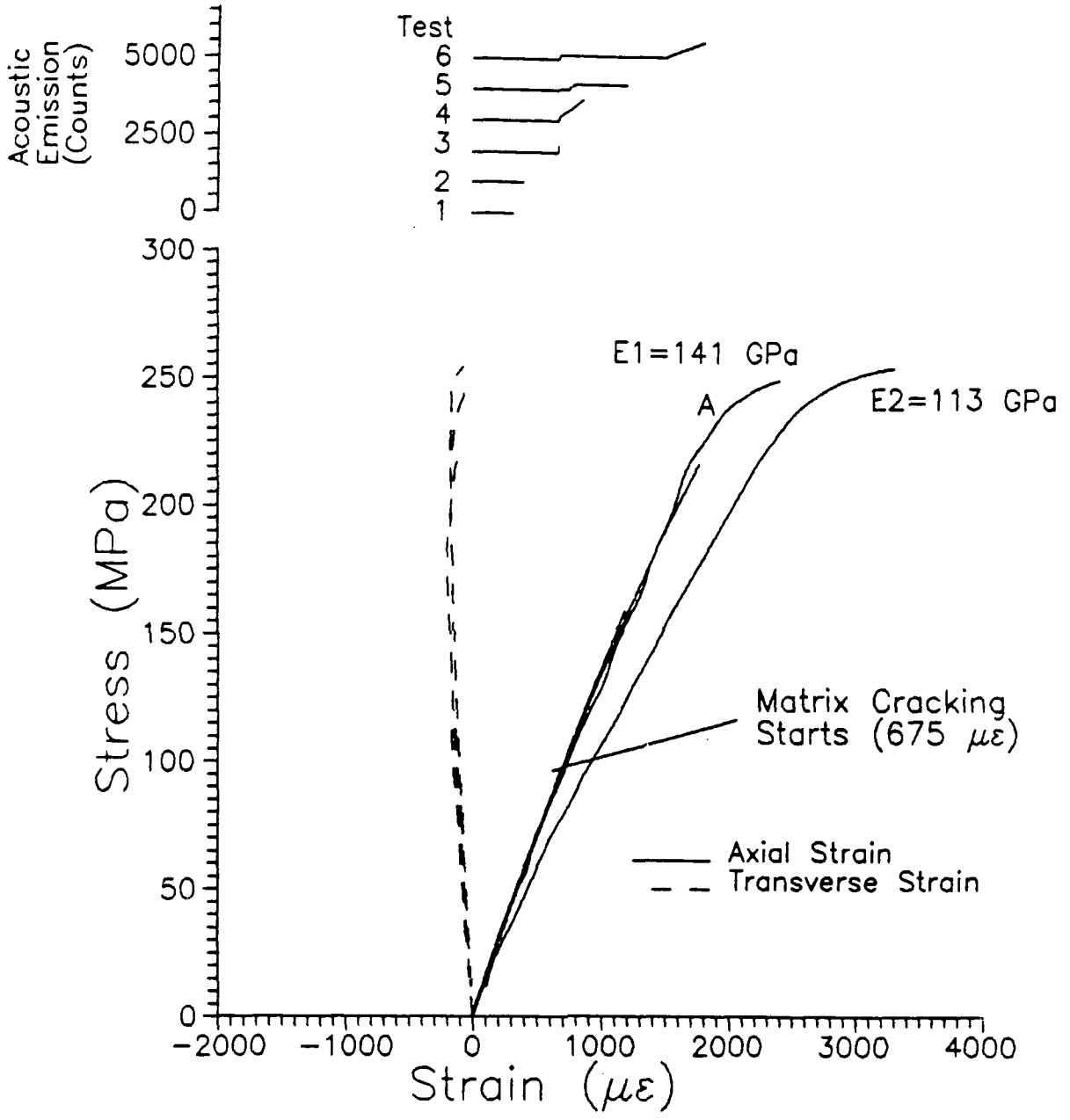

Figure 15 Stress vs Strain and Acoustic Emission for 0 Degree Specimen (0-2) Incremental Loading

and finally loaded to failure. Figure 15 shows that when the specimen was unloaded while the stress-strain curve is linear, the modulus of elasticity does not change. But if it is reloaded after the stress-strain curve had gone nonlinear in the previous test, the modulus was lower and behaved more ductile. This was probably due to fracture of the bond between the matrix and the fiber, leaving the fibers to carry all the load and therefore enabling the less brittle fiber to stretch more. This was also observed by Kim and Pagano (1) for this material.

After the matrix has finished cracking, the fibers begin to break and pull through the matrix. As seen in Figure 16 the failure surface for the 0 degree specimen is perpendicular to the load direction. Figure 16 shows the fracture surface and broken fibers which have pulled out of the matrix. Figure 17 shows the fracture surface perpendicular to the load direction. It could be concluded from these pictures and the above discussion that the bond between the matrix and the fiber was severed before the fibers started breaking and the final failure was due to the fibers failure only. There was little fiber-matrix bonding at ultimate failure, otherwise the matrix fracture would not have been so clean.

2. 15 Degree Specimen

This section will discuss the crack initiation and progression in the 15 degree load specimen. Also the

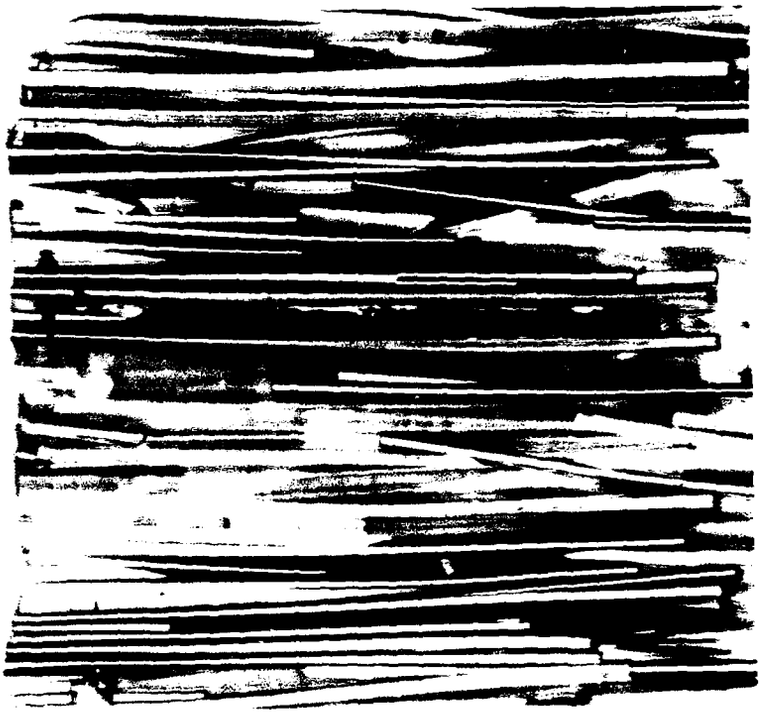

Figure 16 Fracture Surface of 0 Degree Specimen (100x)

(a) Across Width (50x)

(b) Across Thickness (50x)

Figure 17 Fracture Surface across Width and Thickness for 0 Degree Specimen

stress-strain curve is discussed.

The initial cracks, matrix cracking, started at an average value of 70 MPa and 530 $\mu\varepsilon$ for stress and strain respectively. These cracks started during the linear portion of the stress-strain curve as in the case of the 0 degree specimens. The cracks were detected by the acoustic emission transducer. Figure 18 shows a typical stress strain curve and computer generated acoustic emission output for the 15 degree tensile tests.

The first cracks were random, starting along the edge of the edge of the specimen. Figure 19a shows an initial crack at the top-center of the picture starting at a stress of 90 MPa. Shortly after cracking more cracks were seen, they were longer but they did not become continuous across the edge. In Figure 19b, at a stress of 113 MPa, three cracks can be seen along the center portion of the picture. These initial cracks were perpendicular to the load direction along the edge, which would be expected because, as seen by the edge, the fiber direction does not effect the direction of the crack, Figure 19a-b. However, these initial cracks through the width were about 25 degrees off the load direction, see Figure 20.

The average final failure occurred at 125 MPa and 900 $\mu\varepsilon$, and occurred in the upper portion of the gage length. The final fracture surface through the width was 25 degrees off the load direction and 10 degrees off the direction of

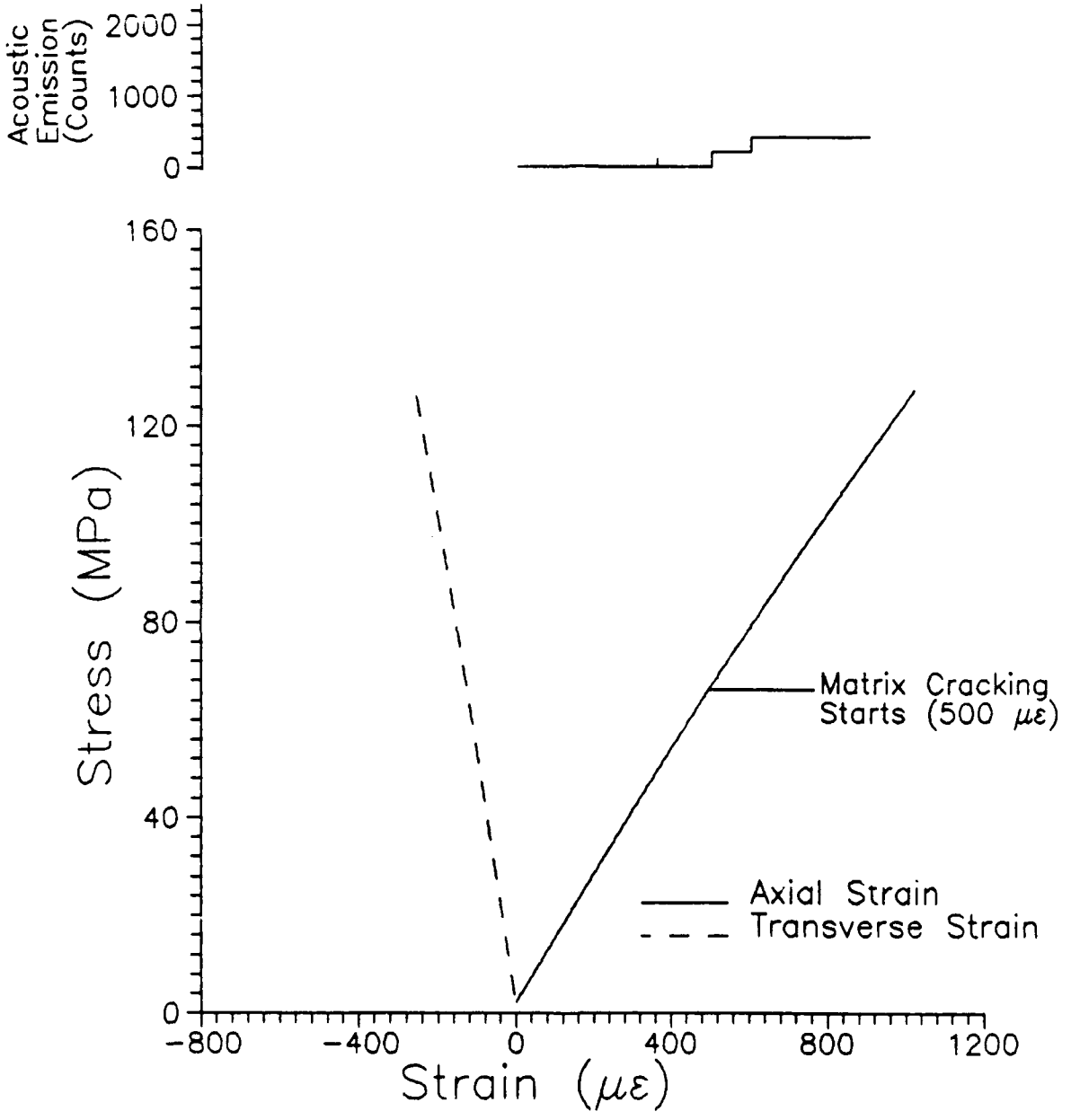

Figure 18 Stress vs Strain and Acoustic Emission for 15 Degree Specimen (15-1)

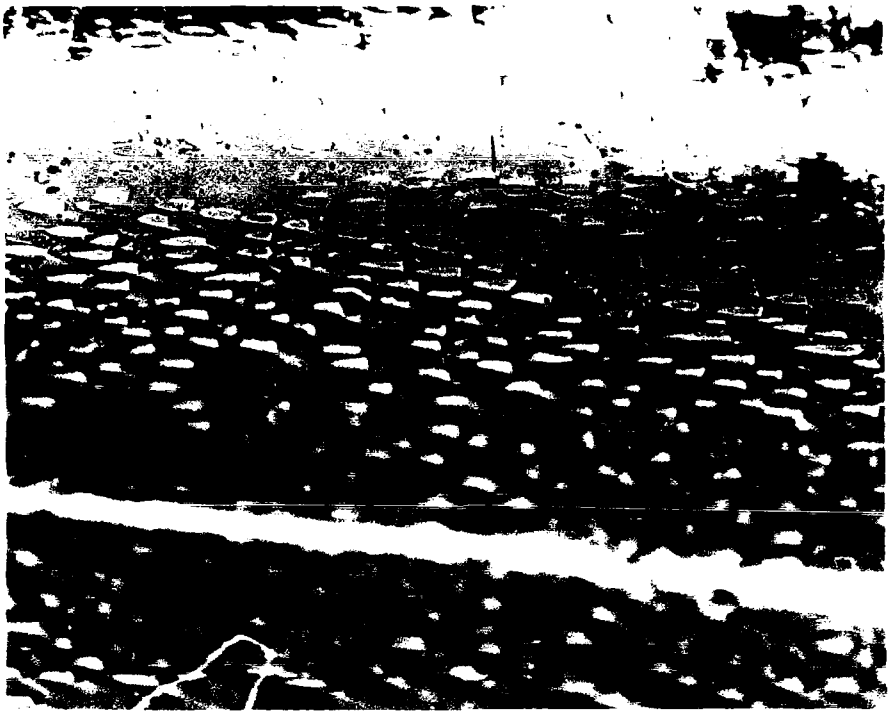

(a) Edge at 92 MPa (100x)

(b) Edge at 113 MPa (100x)

Figure 19 Crack Progression for 15 Degree Specimen

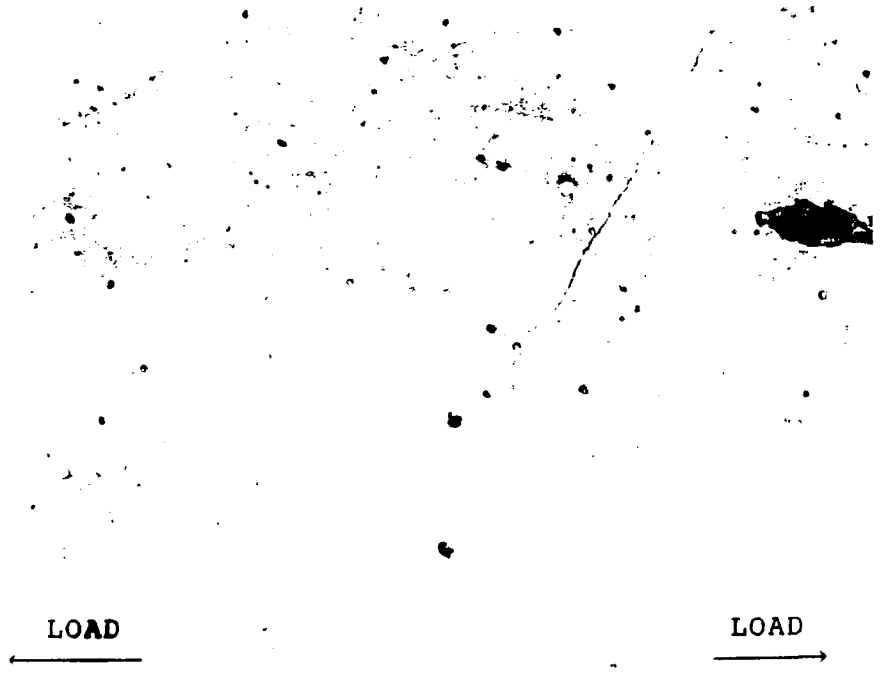

Figure 20 Direction of Initial Crack on Face of 15 Degree Specimen (15-2)

the fibers, as seen in Figures 21 and 22. Notice in Figure 22 the fibers in the specimen are about ten degrees off from the fracture surface. The picture also shows how some fibers are showing along the final crack interface, but not as much as in the 0 degree specimen. This shows that the fibers still carried a part of the load after the matrix starts cracking, and finally broke after some fiber had pulled out.

As mentioned earlier Figure 18 is a typical stress-strain curve. It was linear for the specimens loaded directly to failure. However, as shown in Figures 43 and 44, in the appendix, the incrementally loaded specimen became nonlinear at the end of the final load right before failure. This specimen was loaded and unloaded a total of five times. The modulus of elasticity for the incrementally loaded specimen did not change with any later loadings.

3. 30 Degrees

This section will discuss the crack initiation, progression, and stress strain curve for the 30 degree specimen.

Cracking in the 30 degree specimen did not start until failure of the specimen. Failure of both tested specimens extended into the tab area. The acoustic emission graphics and stress-strain curve are shown in Figure 23. As can be seen the acoustic line is flat, indicating that no cracks were detected before failure.

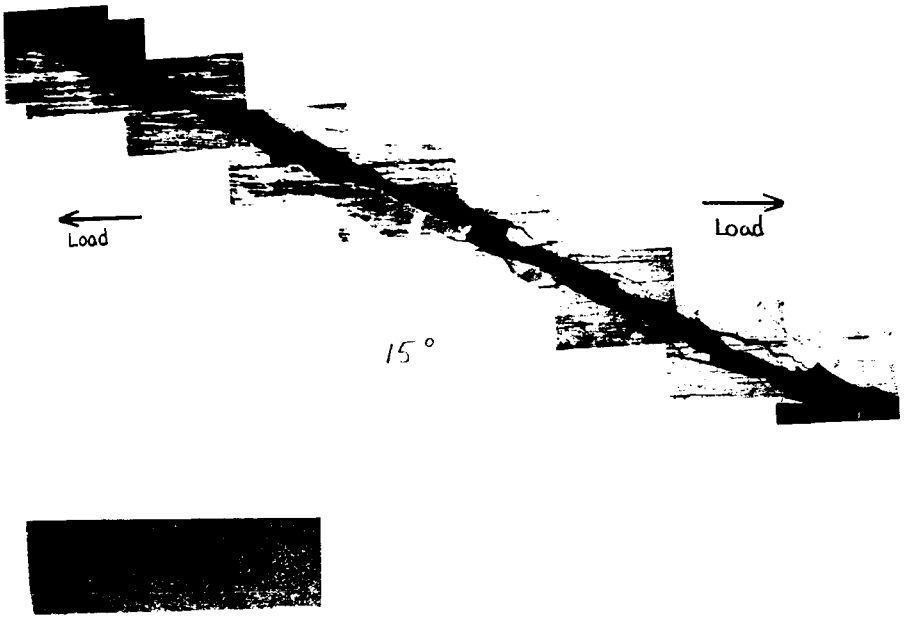

(a) Across Width (50x)

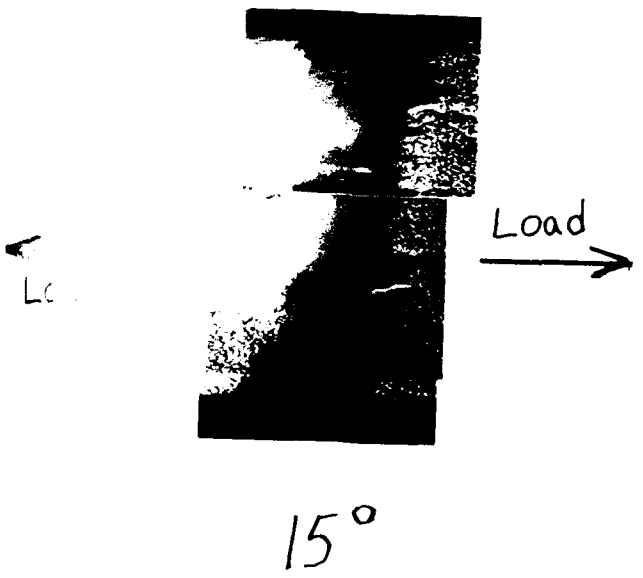

(b) Across Thickness (50x)

Figure 21 Fracture Surface across Width and Thickness for 15 Degree Specimen

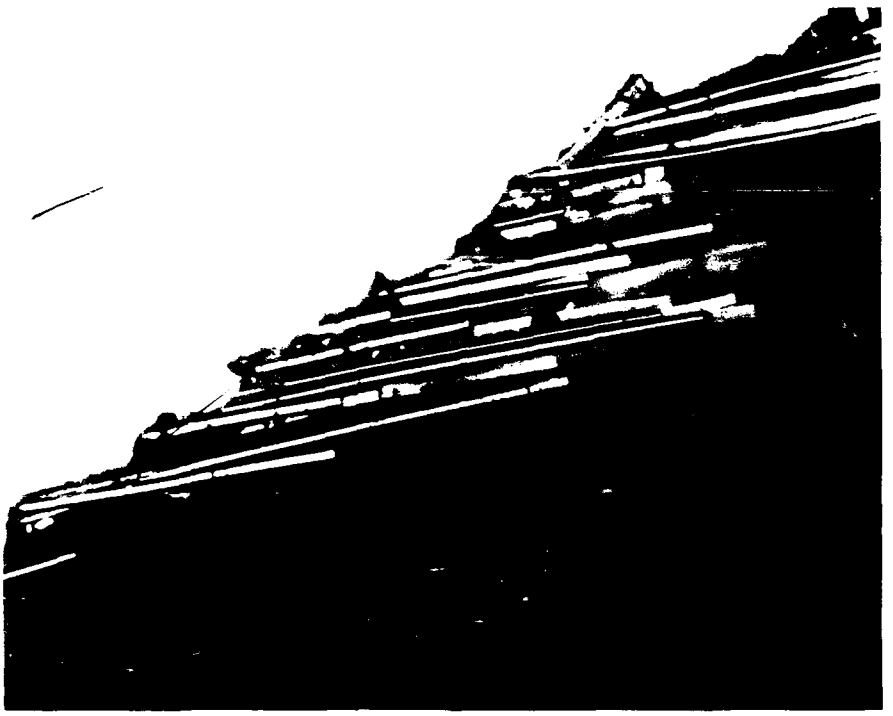

Figure 22 Close-up of Fracture Surface of 15 Degree Specimen (100x)

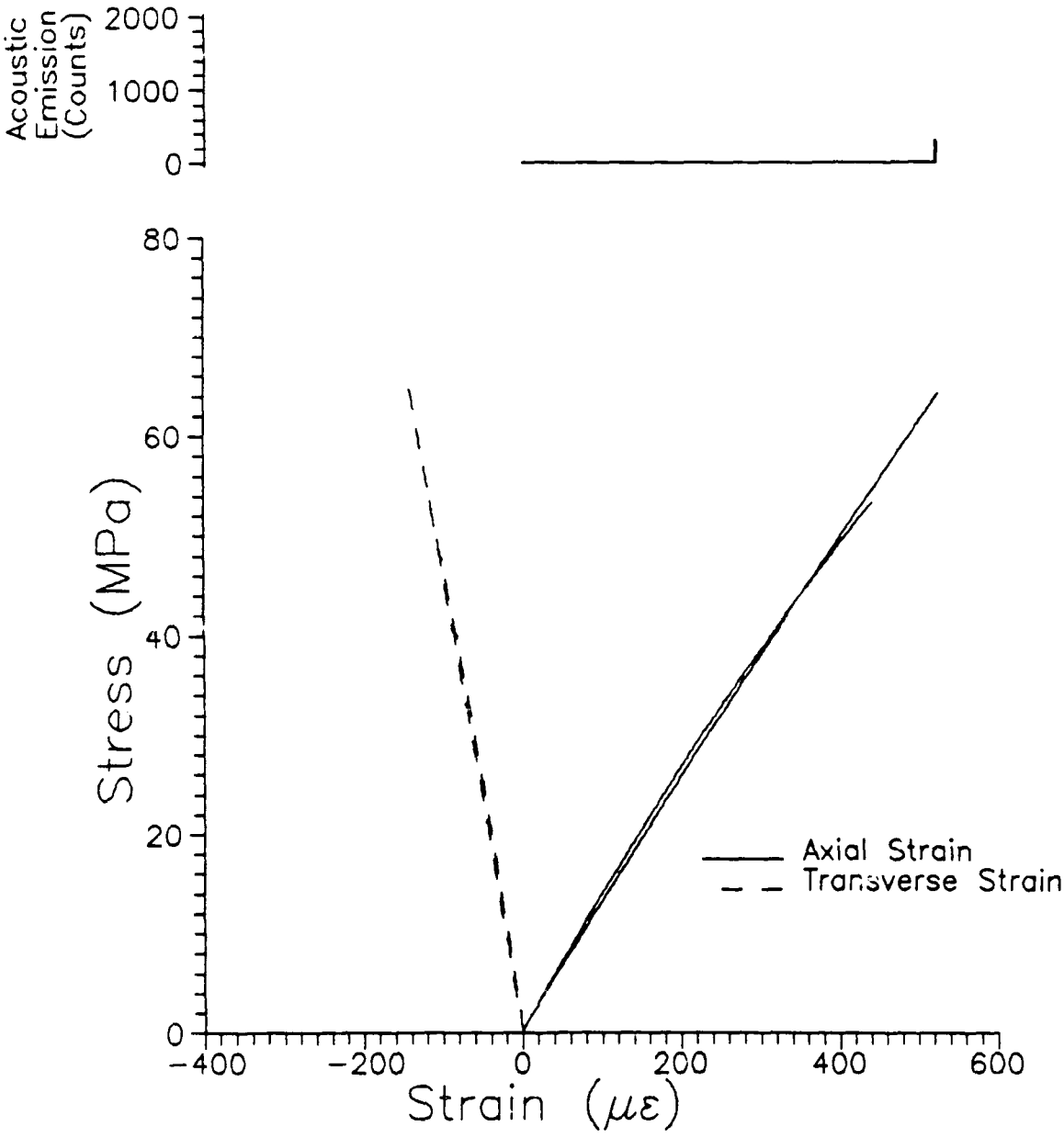

Figure 23 Stress vs Strain and Acoustic Emission for 30 Degree Specimen (30-1) Incremental Loading

The average ultimate stress and strain for this orientation was 72.1 MPa and 576 $\mu\varepsilon$ respectively. The final failure through the width was in the direction of the fibers, 30 degrees off the direction of the load, see Figure 24 and 25. Figure 25 shows minimal fibers protruding from the edge of the final crack interface. This means the fiber did very little of the load carrying after the matrix started to fail.

Only two 30 degree specimens were tested, the third one broke at an unusually low stress probably because of MTS machine grip alignment problems. The first stress-strain curve for the 30 degree specimen is shown in Figure 23. It shows that the stress-strain curve is linear throughout the test. The second test, shown in Figure 26, was loaded and unloaded to four different levels of stress. The figure shows an increase in the modulus of elasticity. This may be caused by the fibers trying to align in the direction of the load. This was the only specimen where this feature was seen and there was not enough material to investigate this phenomena further.

4. 45 Degree

This section will discuss the crack initiation, crack progression, and the stress strain curve in the 45 degree specimen.

The testing of this specimen was very difficult since several of the specimens broke while trying to install them

(a) Across Width (50x)

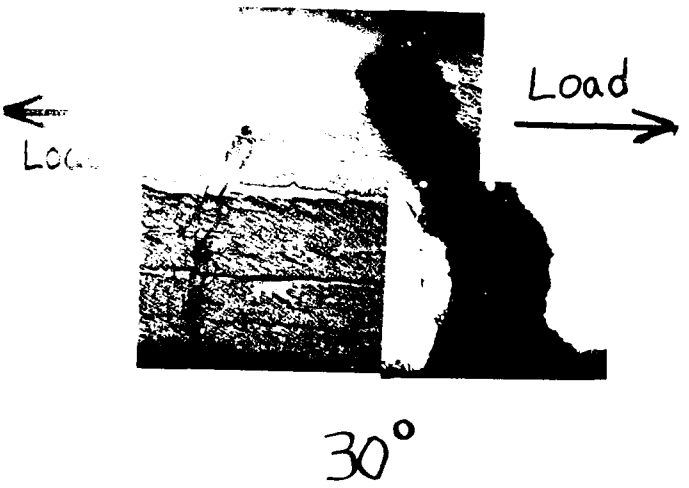

(b) Across Thickness (50x)

Figure 24 Fracture Surface across Width and Thickness for 30 Degree Specimen

Figure 25 Close-up of Fracture Surface of 30 Degree Specimen (100x)

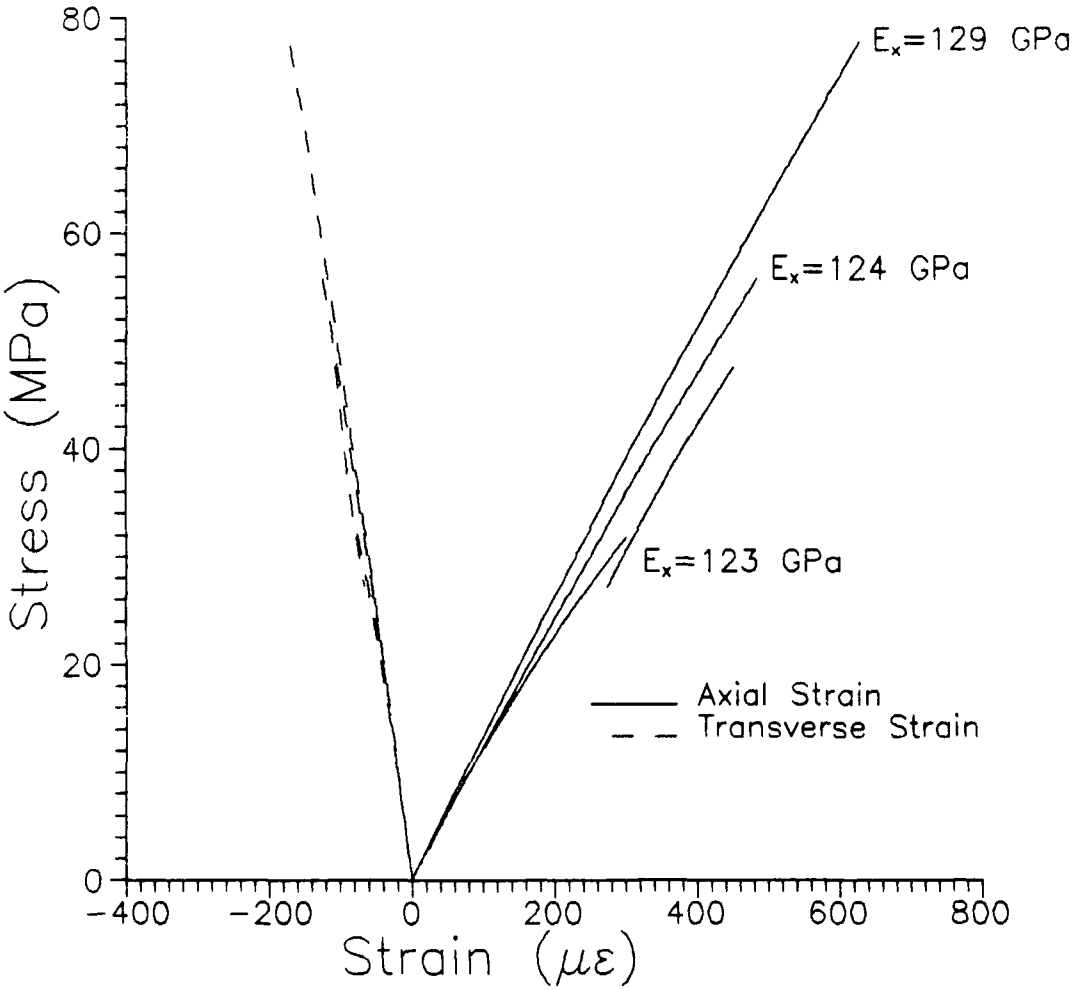

Figure 26 Stress vs Strain for 30 Degree Specimen (30-2) Incremental Loading

in the MTS machine grips. The specimen was too strong to use the mounting fixture as in the 60 and 90 degree specimens. The epoxy would not hold it in the fixture up to failure. And due to the MTS machine grip alignment limitations, they would break when trying to install them in the grips. The only way to get a good test was to align the grips so there was no bending in the specimen. This took a lot of time, effort, and luck to accomplish.

The final failure of the 45 degree specimen usually occurred close to the tab area, extending one side into a very small portion in the tab. Final failure occurred at an average value of stress of 48 MPa and strain of 500 $\mu\varepsilon$. Figure 27 shows its final crack is in the direction of the fiber. Figure 28 shows there are no fibers showing at the fracture surface. This shows the fibers did not carry any of the load after matrix failure.

The stress-strain curves for this specimen were very interesting. The stress-strain curves, for two of the 45 degree specimens (45-5 and 45-7), had two nonlinear areas. Both had the same shape, Figure 29 shows one of these curves. This curve at first is linear, then goes nonlinear at A, goes linear again at B, and finally goes nonlinear again at C. No acoustic emission data was taken during these two tests since the gage length was too small for the acoustic emission transducer and it was expected to fail like the 30 degree specimen. It is suspected that cracking

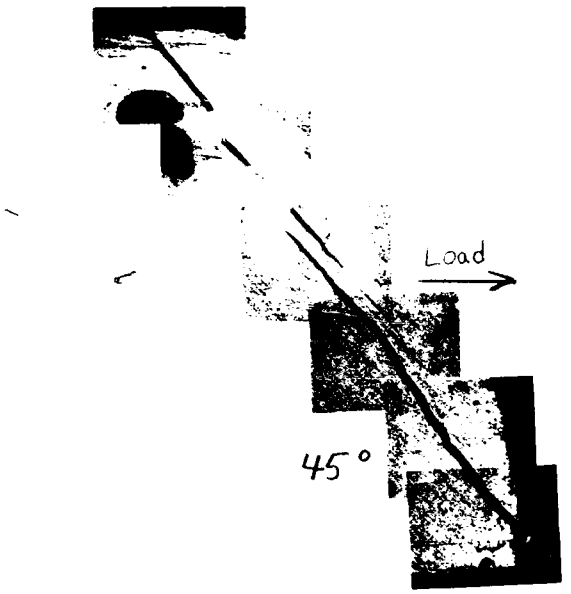

(a) Across Width (50x)

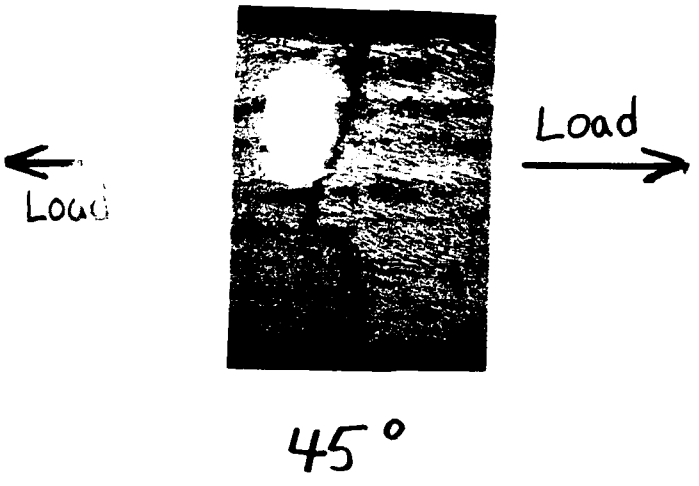

(b) Across Thickness (50x)

Figure 27 Fracture Surface across Width and Thickness for 45 Degree Specimen

Figure 28 Close-up of Fracture Surface of 45 Degree Specimen (100x)

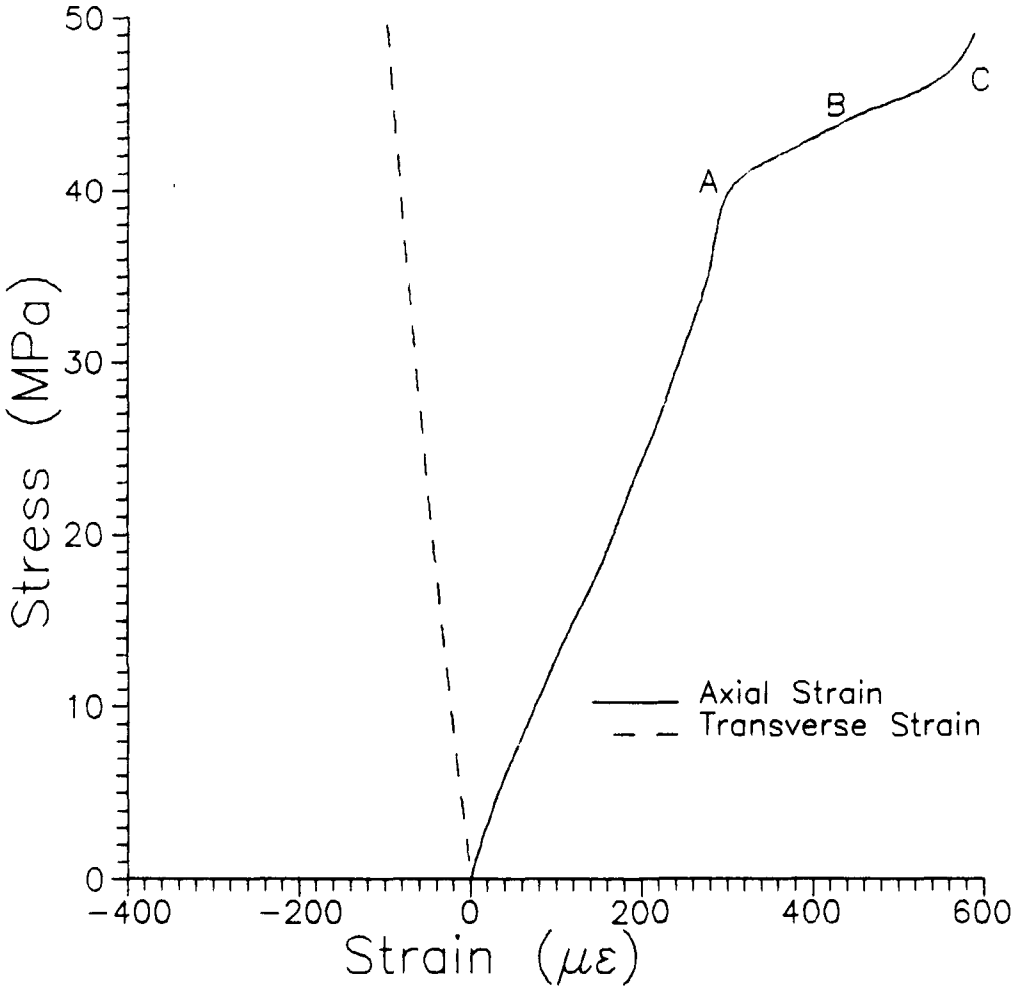

Figure 29 Stress vs Strain for 45 Degree Specimen (45-5)

occured when the stress-strain curve became nonlinear. During the flat portion at B the tabs added extra strength to the specimen due to the short gage length. And also, because the fracture surface started to enter the tab. The other specimen's (45-8) stress-strain curve was linear until failure, as shown in Figure 30. Specimen 45-8 was loaded incrementally, 4 different load levels, to try and detect matrix cracking. Further, in test 45-8, acoustic emission was used and no cracking was detected. There was not enough material to study this phenomena any further.

5. 60 Degree

Cracking in the 60 degree specimen did not start until final failure of the specimen. The final failure through the width was in the direction of the fibers 60 degrees off the direction of the load, as shown in Figure 31. The average values for ultimate stress and strain are 26.6 MPa and 247 $\mu\varepsilon$ respectively.

The stress-strain curve was linear until failure, see Figure 32. Three specimens were incrementally loaded to try and detect matrix cracking. There was no matrix cracking before failure. Acoustic emission did not detect anything until failure.

6. 90 Degree

Cracking in the 90 degree specimen did not start until failure of the specimen. The final failure through the width was in the direction of the fibers 90 degrees off the

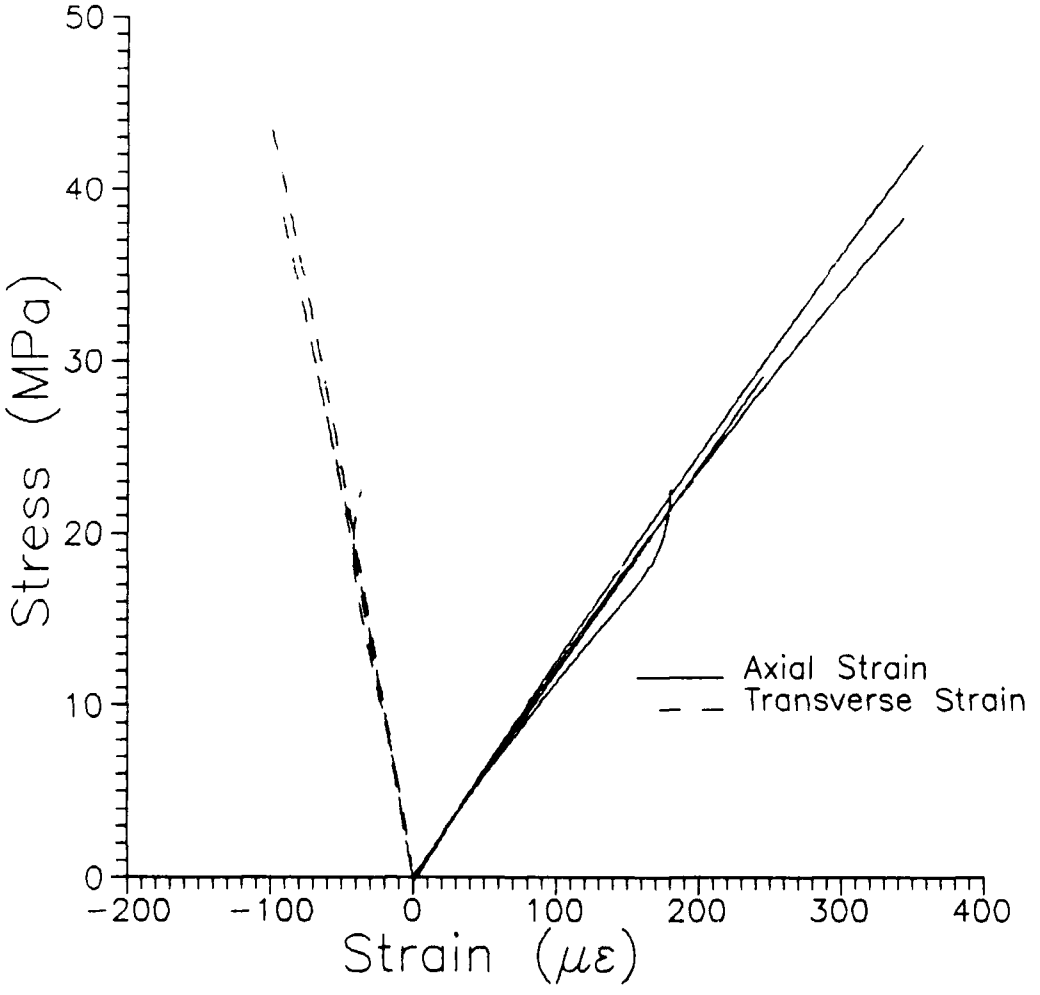

Figure 30 Stress vs Strain for 45 Degree Specimen (45-8) Incremental Loading

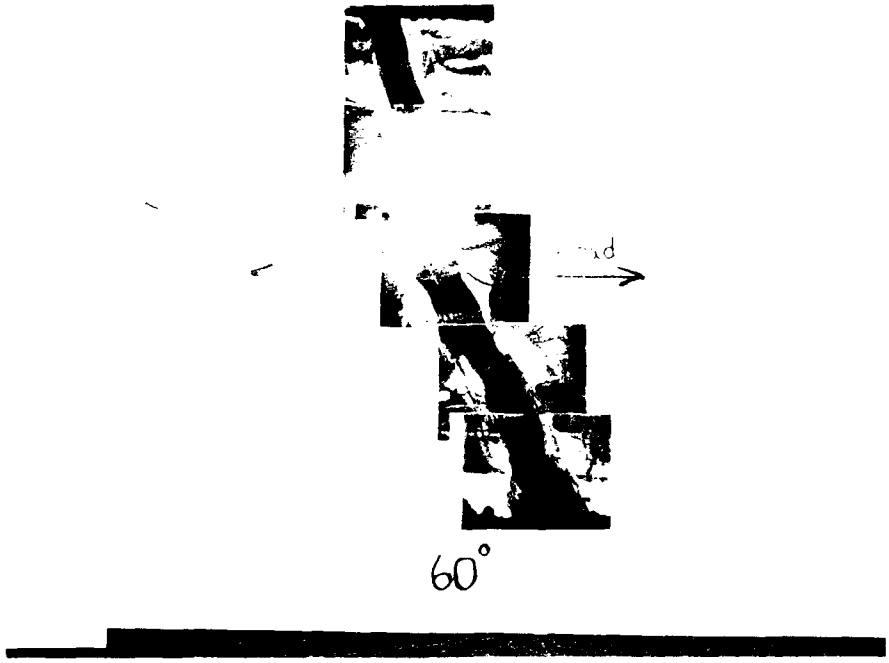

(a) Across Width (50x)

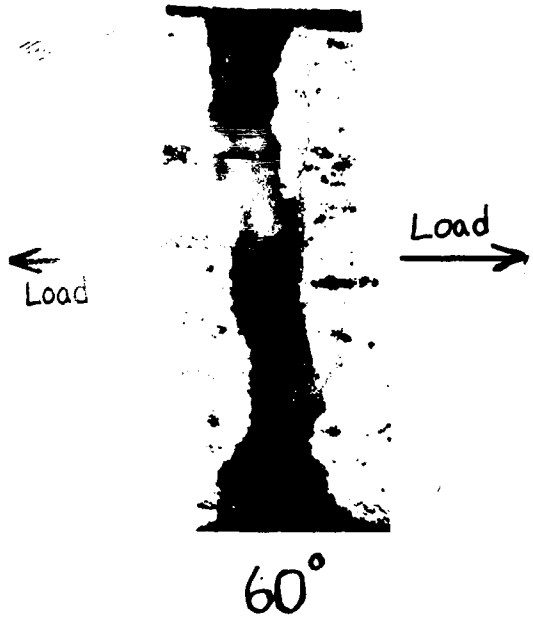

(b) Across Thickness (50x)

Figure 31 Fracture Surface across Width and Thickness for 60 Degree Specimen

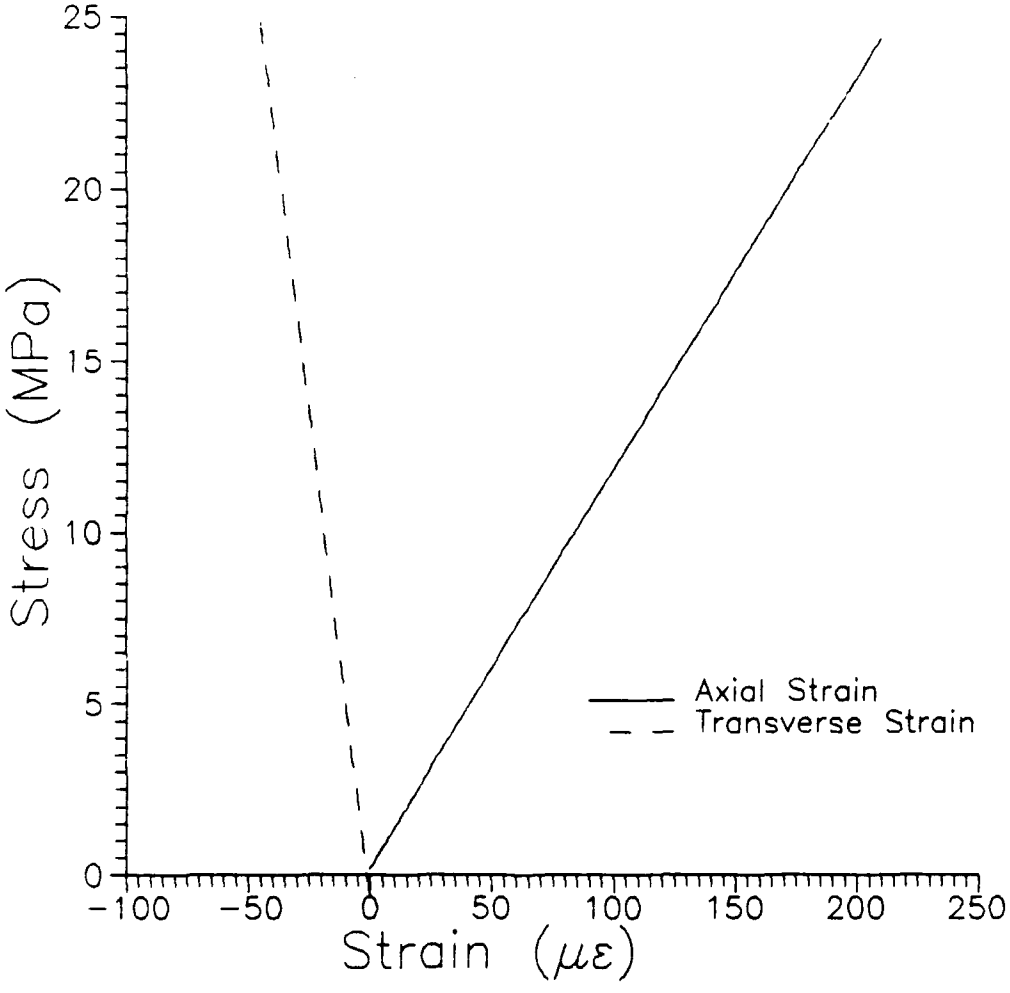

Figure 32 Stress vs Strain for 60 Degree Specimen (60-1) Incremental Loading

direction of the load, see Figure 33. There was no fiber showing at the fractured surface. The average failure stress and strain occurred at 19.1 MPa and 217 $\mu\varepsilon$ respectively.

The stress-strain curve was linear until failure, see Figure 34. There were no incremental loadings of the 90 degree specimen, since the specimen was so fragile and the failures were straight forward.

7. Overall Observations

All the off-axis specimens failed in the direction parallel to the fibers, except for the 15 degree specimens which failed at 25 degrees off the load direction, see Figure 35. Cracking in the 0 and 15 degree loaded specimens starts in the matrix during the linear portion of the stress-strain curve. The 45 degree loaded specimens probably cracked before failure when the stress-strain curve became nonlinear but this could not be confirmed due to limited testing material. The 30, 60, and 90 degree specimens showed no matrix cracking before failure nor nonlinearity in their stress-strain curves. Transverse strain reversal was seen in the 0 degree specimen (4), but not in any of the other load orientations.

C. Theoretical Models

This section will compare the test results with the theoretical models outlined in Chapter II. The E_1, and E_2

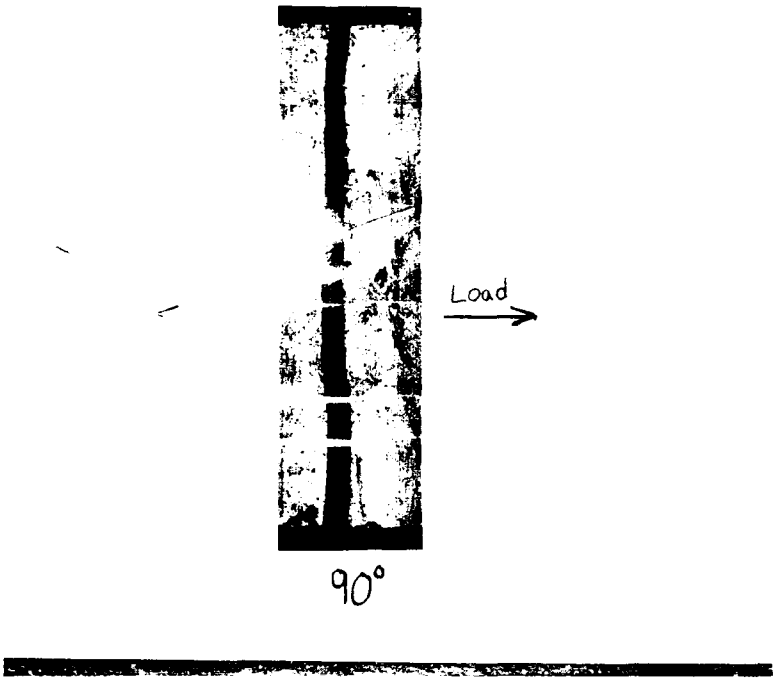

(a) Across Width (50x)

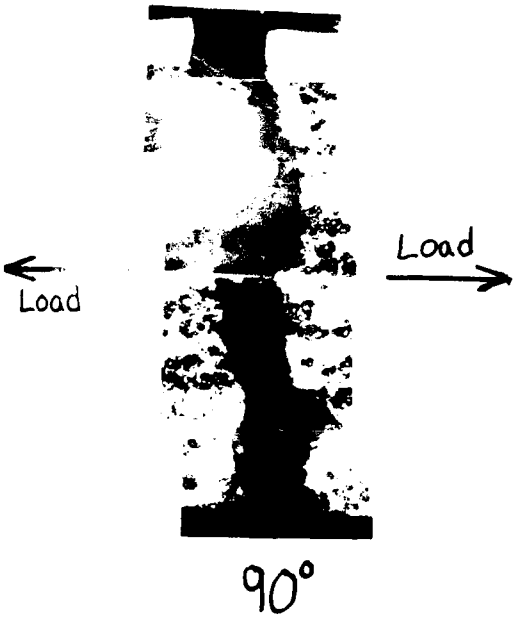

(b) Across Thickness (50x)

Figure 33 Fracture Surface across Width and Thickness for 90 Degree Specimen

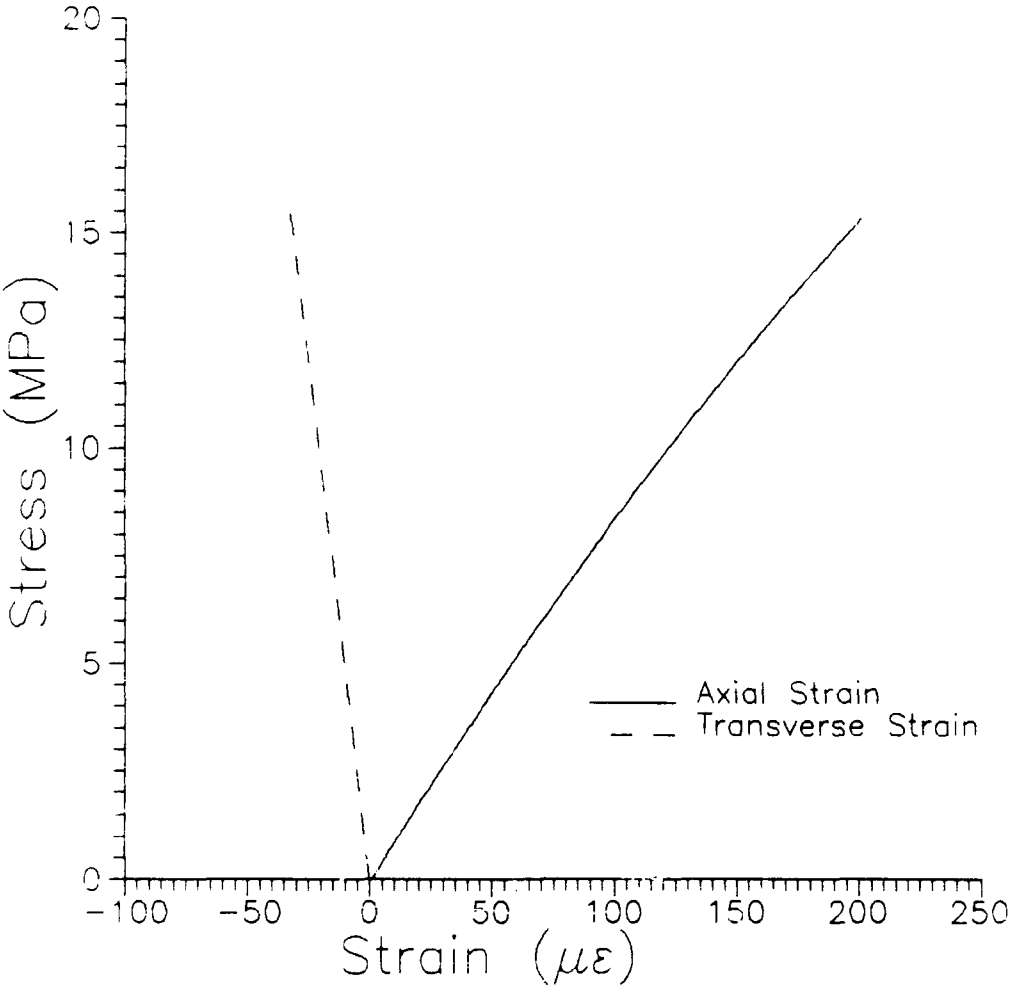

Figure 34 Stress vs Strain for 90 Degree Specimen (90-4)

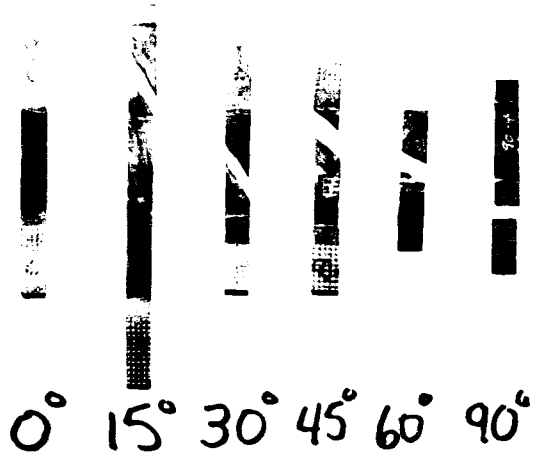

Figure 35 Broken Specimens for each Off-axis Load Orientation

models will be used to try and understand the fiber-matrix interface properties. The E_x, ν_{xy}, and failure criteria models will be compared with the test data to see if these models can be used to predict the behavior of the ceramic composite in off-axis loading. And finally, the crack density model will be compared with test data.

1. Principal Direction Modulii from Theoretical Models

This theory will show that there was some bonding between the fiber and matrix in the tested ceramic composite. But this bond was not perfectly elastic.

Using the rule of mixtures, equation (1), the axial modulus can be predicted. Using the values for the matrix and fiber in Table 1, page 19, the predicted value for E_1 is 132 MPa, this compares very well with the test value of 139 MPa. This is not surprising since the fibers carry most of the load and they are continuous through the load direction. If the fiber contribution was zero, E_1 would be equal to 64.6 MPa which is almost half of the tested value. According to Bhatt and Phillips (7), this shows that E_1 for this material behaves like there is an elastic bond between the fiber and the matrix. Bhatt et al showed the same results for SiC/RBSN. The rule of mixtures can be used to predict E_1 in this type of material.

The transverse modulus is more difficult to predict. For a well bonded composite E_2 can be predicted using the Halpin-Tsai equation, eqn (2), and for a weak bond it can be

predicted using the Halpin-Tsai equations modified by Bhatt et al (7), eqn 4, both are outlined in Chapter II.

If the tested composite had a perfect bond between the matrix and fiber, the Halpin-Tsai equation predicts E_2 to be equal to 126 GPa. The tested value for E_2, however, was 96.7 GPa. The well bonded prediction is 30 percent higher than the tested value. The modified Halpin-Tsai equations for the weak bonded system, which assumes no contribution from the fiber, predicted E_2 to be 55 GPa. This is 40 percent less than the tested value (96.6 GPa). Therefore, this type of ceramic composite does not have a perfectly elastic bond between the matrix and the fiber, but does have appreciable bonding. The Halpin-Tsai and modified Halpin-Tsai equations can, therefore, be used to predict the upper and lower limits of the transverse modulus for this type of composite.

2. Theoretical Models for Modulus and Poisson's Ratio in Off-axis Loading.

This section will compare the off-axis loading test results for E_x and ν_{xy} with the present theory, see chapter II equations (15 and 16). The theory assumes an orthotropic material in plane stress. The theory predicts E_x and ν_{xy} for off-axis loading given E_1, E_2, ν_{12}, and G_{12}. The first three properties were obtained from test results of the present study. The last, G_{12}, was calculated using equations (15 and 16) and the following given test data:

a. 15 degree test data for E_x and ν_{xy}

b. 0 degree test data for E_1 and ν_{12}

c. 90 degree test data for E_2

G_{12} was calculated to be 44 GPa.

Figure 36 shows a comparison of the theoretical model and the test data for E_x. The theoretical model predictions for E_x, using eqn (15), are shown as the solid line. The test results outlined in Table 2 are plotted in Figure 36 as circles. The vertical lines going through the circles show the scatter of the test data. As can be seen the theoretical predictions are within the scatter of the data. The data also show the same trends as the theory predictions. The maximum deviation occurred at 60 degrees where the prediction was 12 percent lower than the test results average.

Figure 37 compares the theoretical predictions and the test data for ν_{xy} during off-axis loading. Using equation (16) the theoretical predictions are shown as a solid line in the figure. The test results outlined in Table 2 are plotted in Figure 37 as circles. The vertical lines going through the circles show the scatter of the test data. As can be seen the average test results show the same trend as the theoretical predictions. It is very hard to get good values for ν_{xy}. They are obtained from the data by taking the slopes of the axial and transverse stress-strain curves and dividing the transverse by the

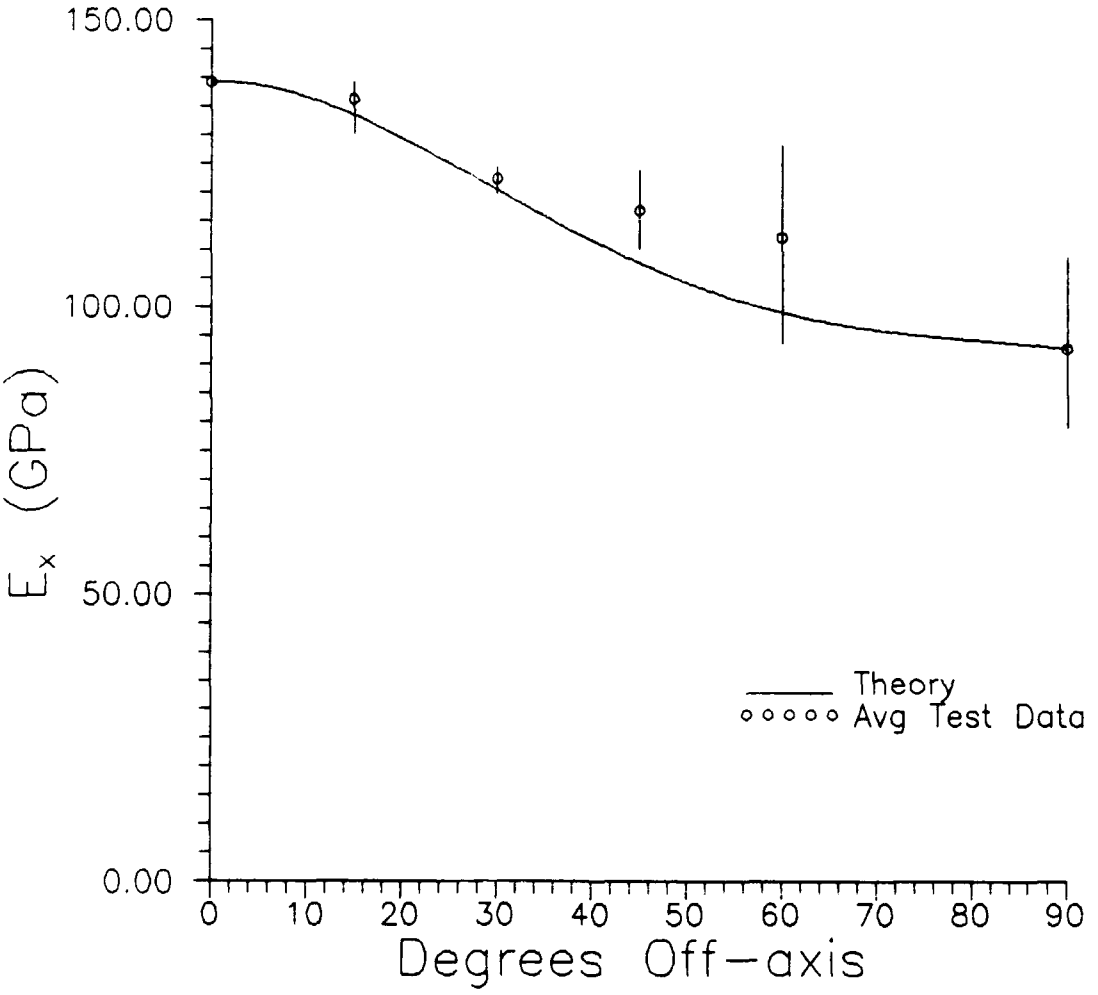

Figure 36 Modulus of Elasticity (E_x) vs Degrees Off-axis Theory and Test Data Comparison

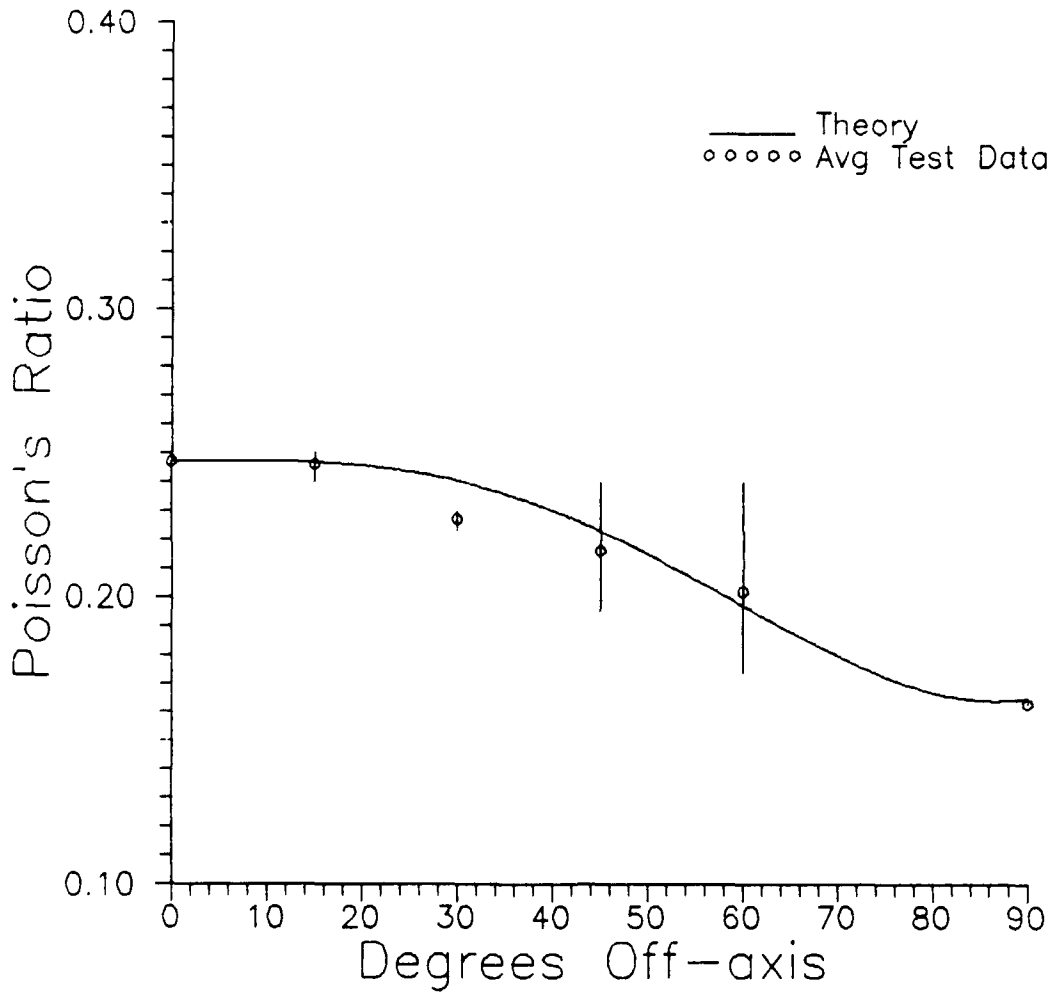

Figure 37 Poisson's Ratio (ν_{xy}) vs Off-axis Degrees Theory and Test Data Comparison

axial. This is not accurate since both slopes were drawn by hand through the respective curves. The maximum difference between the theoretical and experimental value is at 30 degrees where the prediction is 6 percent high.

3. Failure Criteria Models.

This section will compare test results with the Tsai-Hill failure model outlined in Chapter II equation (31). This model predicts the failure stress of a composite in off-axis loading from the available failure stresses in the 1 and 2 direction and shear. This model assumes the tensile and compression strengths are the same for the composite. Two different definitions for failure criteria were considered. Firstly, the ultimate stress will be considered for the failure criteria. Secondly, the start of matrix cracking will be considered as the failure criteria.

a. Ultimate Strength.

The theoretical predictions were calculated using eqn (31) and the following data:

(1). X - 0 degree average ultimate stress test data (266 MPa).

(2). Y - 90 degree average ultimate stress test data (19.1 MPa).

(3). S - material specification supplied by Corning Glass Works (38 MPa).

Figure 38 show the comparison of theoretical predictions to the test results. The predicted values for

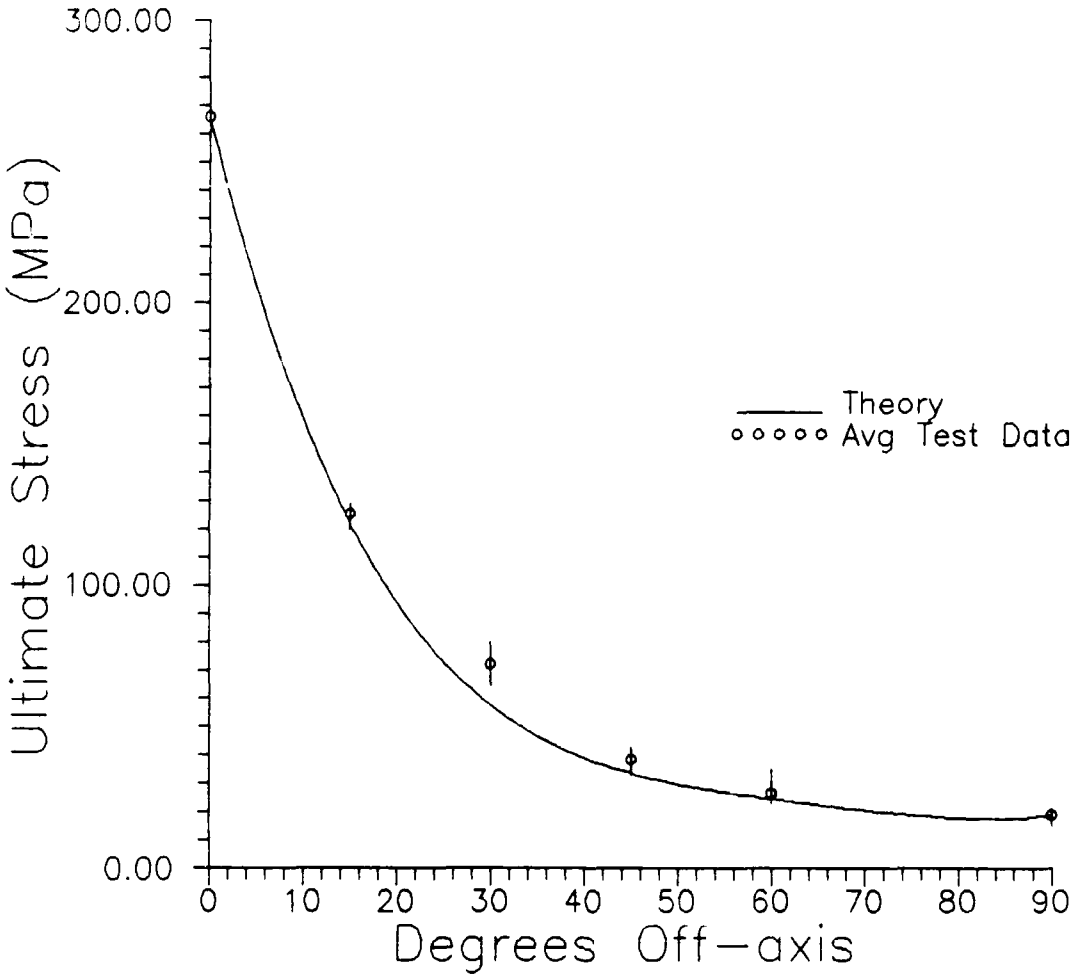

Figure 38 Ultimate Stress (σ_x^{ult}) vs Degrees Off-axis Tsai-Hill Model and Test Data Comparison

off-axis loading are shown as the solid line. The test results, tabulated in Table 2, are shown in Figure 38 with the average value as a circle. The vertical line in the figure shows the scatter of the test data. The maximum deviation occurred at 30 degrees and the prediction is 20 percent lower than the test results. Figure 38 shows that the Tsai-Hill failure criteria can be used to approximate the ultimate failure in this ceramic composite.

b. Matrix Cracking.

Since the start of damage to a material is very important to researchers and designers. This section will discuss the use of Tsai-Hill failure criteria to predict the start of matrix cracking in off-axis loading.

The average value of the 0 degree matrix cracking stress, σ_x^{mc} (from Table 2), was used for X in eqn (31). The average value for the 90 degree ultimate stress was used for Y. The shear stress S was calculated using eqn (31) and solving for S using the following data:

(1). $\sigma_x = \sigma_x^{mc}$ at 15 degrees from Table 2 (test results)

(2). $X = \sigma_x^{mc}$ at 0 degrees from Table 2

(3). $Y = \sigma_x^{ult}$ at 90 degrees from Table 2

S was calculated to be 29.2 GPa.

Figure 39 compares the predicted values for the matrix cracking stress to the test data tabulated in Table 2. The solid line shows the predicted results. The average value for matrix cracking at each load orientation,

from Table 2, is shown in the figure as circle. The vertical line shows the scatter of the data. In Figure 39 the predicted values compare well with the test data except for the 30 degree matrix cracking. The theory goes through all the scatter bars except for the 30 degree data. Possibly the matrix cracking was missed in the 30 degree tests. There were only 2 good data points for this material and not enough material to test further. However, the incrementally loaded specimen was tested to 4 different load level, and no cracks were found before failure. Another possibility is there is a different failure criteria driving the failure, such as maximum strain in the 2 direction (transverse principal axis).

Sensitivity of the predictions due to the scatter of the 0 and 90 degree test data are shown in Figures 40 and 41. Figure 40 shows the sensitivity of the theory due to the upper and lower values of the 0 degree matrix cracking data (X in eqn 31). The upper dashed line shows the prediction using the highest point of data and the lower dashed line for the lowest. And Figure 41 shows sensitivity of the theory to the upper and lower values of the 90 degree matrix cracking data (Y in eqn (31)). The upper and lower dashed lines are the same as for the previous figure. These two figures show that all the test data averages, except the 30 degree data, fall within the scatter band of the theoretical model. Thus, the scatter

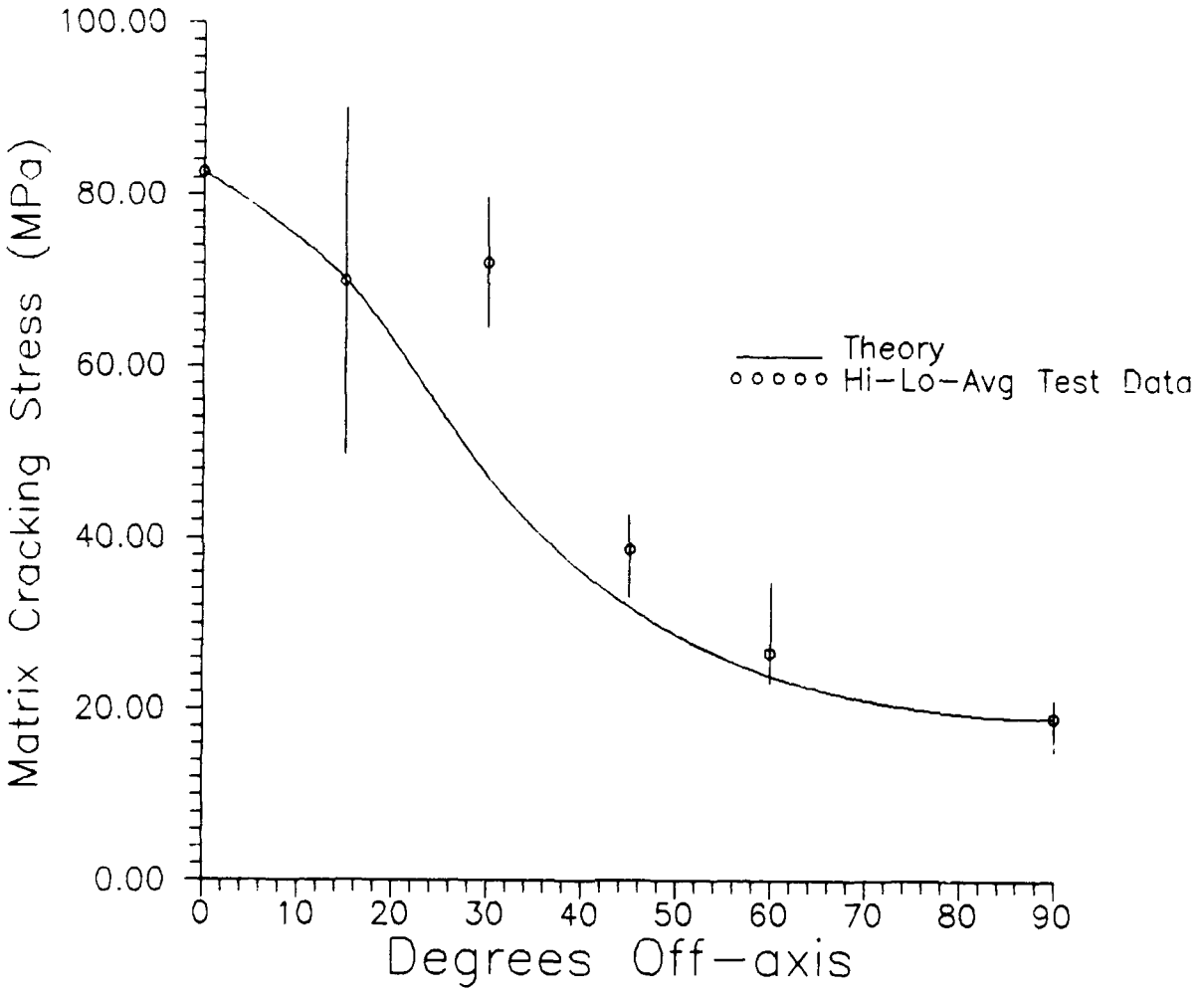

Figure 39 Matrix Cracking Stress (σ_x^{mc}) vs Degrees Off-axis
Tsai-Hill Model and Test Data Comparison

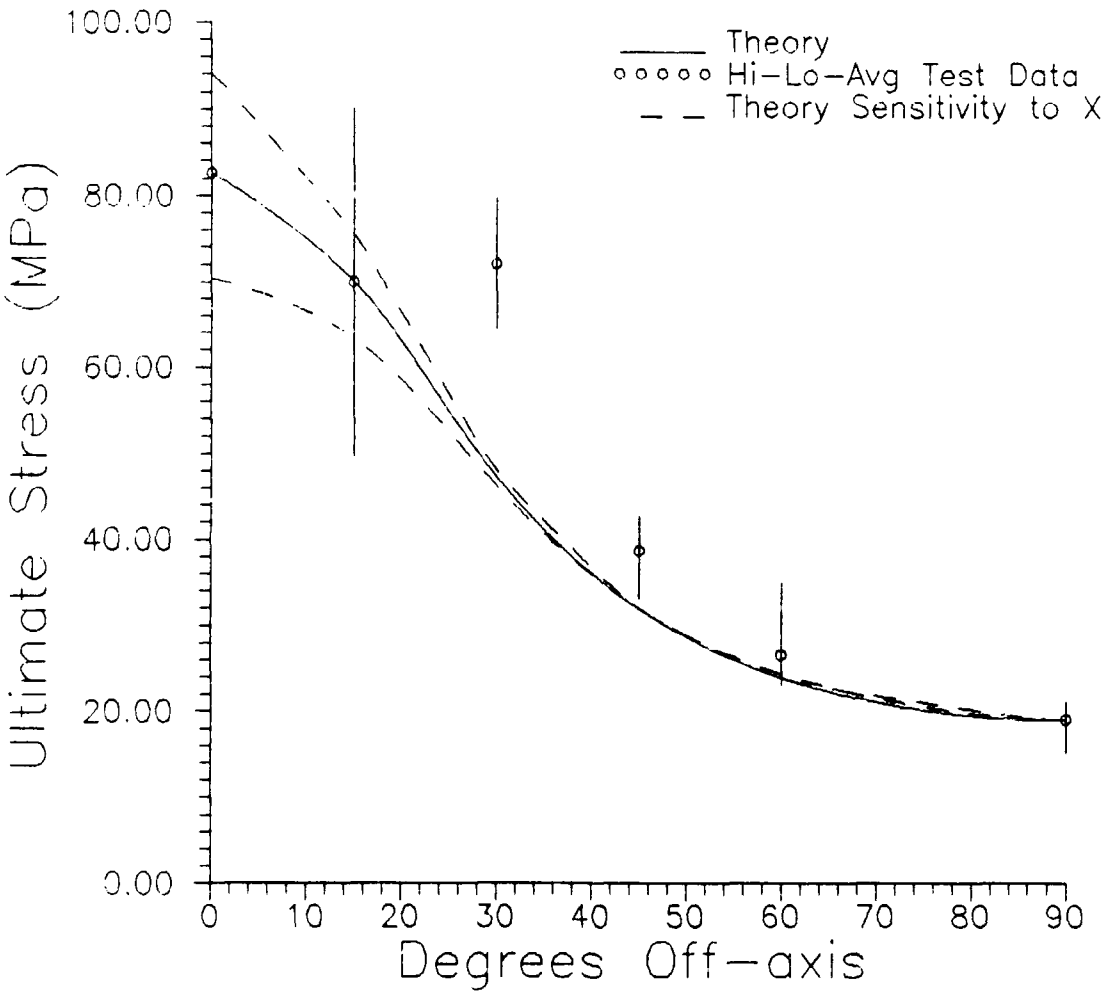

Figure 40 Matrix Cracking Stress (σ_x^{mc}) vs Degrees Off-axis
Tsai-Hill Model and Test Data Comparison
Sensitivity to 0 Degree Data Scatter

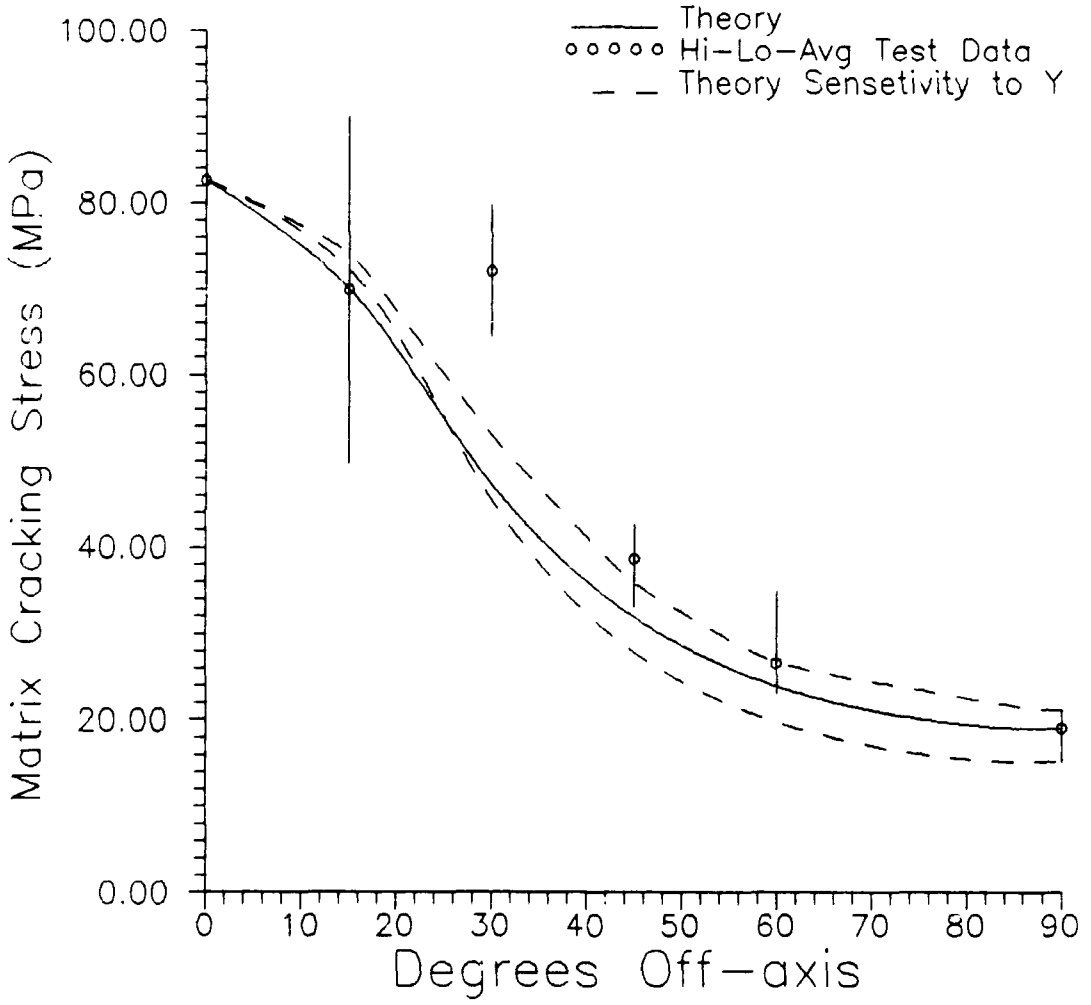

Figure 41 Matrix Cracking Stress (σ_x^{mc}) vs Degrees Off-axis
Tsai-Hill Model and Test Data Comparison
Sensitivity to 90 Degree Data Scatter

can not account for the deviation in the 30 degree data from the theory. Hence, it can be concluded that onset of matrix cracking in this ceramic composite can be predicted accurately by this method except for the 30 degree load orientation. However, this does need further investigation due to the limited 30 degree test data.

4. Crack Density.

Ceramic composites have shown a property where a minimum crack spacing is reached before failure of the material. Aveston, Cooper, and Kelly (11) formulated a theory to predict the minimum crack spacing for a well bonded composite material, as outlined in Chapter II.

Using the Aveston et al theory for a elastically bonded matrix fiber composite the minimum crack spacing for this material would be between (5 μm and 10 μm). The minimum crack spacing found during this testing was 107 μm. Marshall and Evans (3) observed a crack spacing of 400 μm in a similar material, SiC/LAS. According to Daniel et al (2) the order of magnitude difference between the minimum crack spacing of the two materials may be because the SiC/LAS material has no bonding between the fiber and the matrix and SiC/CASII does have some bonding but does not have a perfectly elastic bond.

The crack density progression was measured at different load levels. At the lower load levels cracking was random and the crack spacing was large. At these levels the crack

spacing was calculated by measuring the length of a replica, counting the number of cracks across the length and dividing the length of the replica by the number of cracks. For the later loadings, when crack spacing was a lot closer, a picture of the replica was taken at one spot and the number of cracks counted and divided into the actual length of the area pictured.

Figure 42 shows, for a 0 degree specimen, the axial stress-strain curve and stress versus normalized crack density. The normalized crack density is the average diameter of the fibers (d), 12.7 μm, divided by the crack spacing (cs). The solid line in the figure is the axial stress-strain curve. The circles are the test data points for the normalized crack density. The dashed line show the trend for the normalized crack density. As was mentioned earlier the initial cracking was randomly distributed. This was observed at the first three points at the left of Figure 42, where the crack density is low. Notice that the matrix cracking starts at a very low stress level and in the linear portion of the stress-strain curve. Once a stress of 218 MPa was reached the crack density increased quickly. The cracking became continuous and had consistent spacing between the cracks. Finally at a stress of 250 MPa the matrix cracking stopped and, soon after, the specimen failed. At this point the minimum crack spacing was 107 μm. Daniels et al (2) found the same trend for the normalized crack

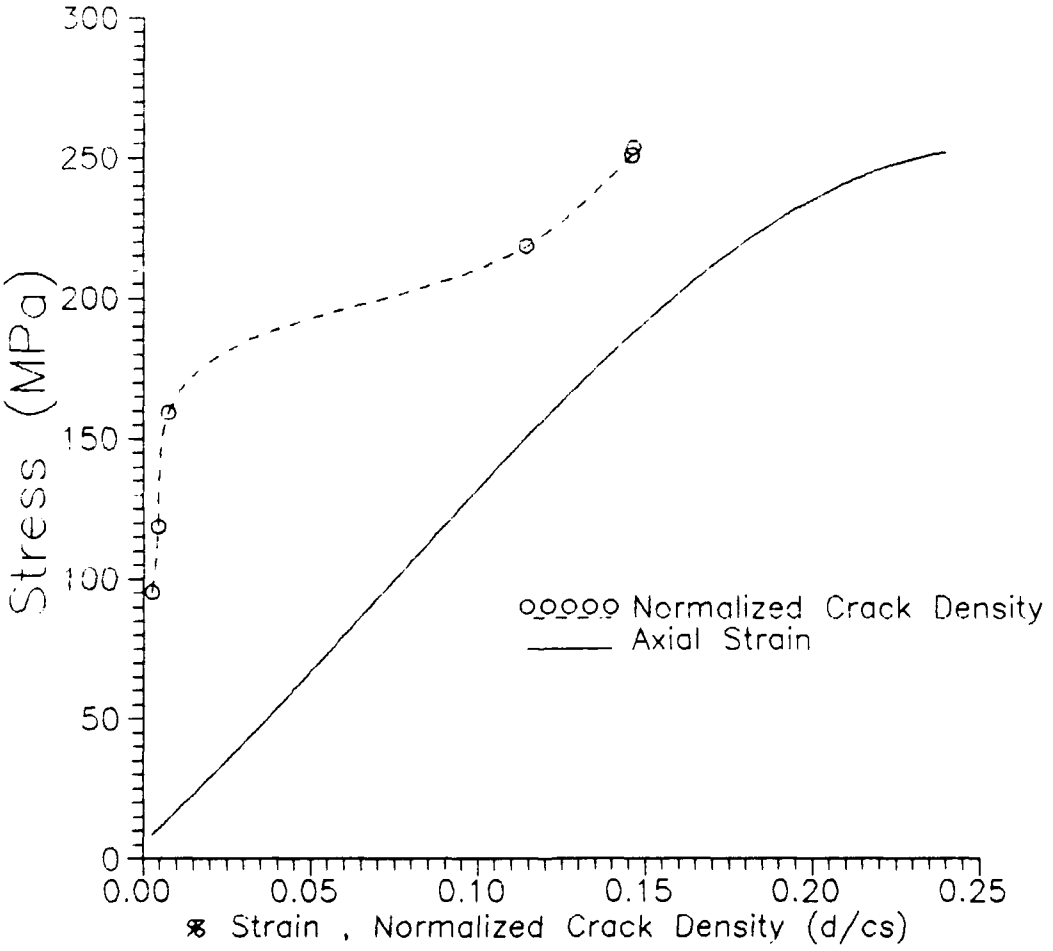

Figure 42 Stress vs Strain, and Stress vs Normalized Crack Density for 0 Degree Specimen

density.

The crack density was very hard to measure and it was not completely tested here, due to the limited amount of material available. For a better understanding of this, the crack spacing samples need to be taken closer together. The continuous cracking seems to take place in a very short interval and happens when the nonlinear portion of the stress-strain curve starts. Further, this crack density phenomenon could be seen only in the 0 degree specimen. No other orientation provided such information.

V. Conclusions

A study was conducted to investigate the initial damage and damage progression in a ceramic composite due to off-axis loading, and compare test data to the available theories of strength and material properties of a polymeric composites in off-axis loading. There is potential for ceramic composites in high temperature applications. A good understanding of this materials characteristics in off-axis loading is required before designers can reliably predict their strength and design life. The composite panel was fabricated by Corning Glass Works. The material was tested in tension on an MTS machine in six different off-axis loadings, 0, 15, 30, 45, 60, and 90 degrees. Acoustic emission was used to initially monitor the initiation of matrix cracking with replication to confirm the cracking. Replication was used to monitor the progression of the damage. Finally the experimentally determined values for strength, material properties, and cracking properties were compared to predicted values from present theories. The conclusions drawn from this study are as follows:

1. In this material acoustic emission is a reliable method for finding the onset of matrix cracking. This was verified by taking replications which should be used while

the load is still applied to the specimen.

2. Cracking in the 0 and 15 degree off-axis loading starts in the matrix during the linear portion of the stress-strain curve. The 45 degree off-axis loading probably cracked before failure when the stress-strain curve became nonlinear but could not be confirmed due to limited testing material. The 30, 60, and 90 degree specimens showed no matrix cracking or nonlinearity in their stress-strain curves.

3. All off-axis loading specimens failed in the direction parallel to the fibers, except for the 15 degree specimens which failed 25 degrees off the direction of the load.

4. Transverse strain reversal was seen in the 0 degree specimen. This was first seen by Kim and Katz (4).

5. There is some bonding between the matrix and fibers. The bond is not perfectly elastic. This was shown from the crack density theory by Aveston et al (11) and the modified Halpin-Tsai equations by Bhatt and Phillips (7). This was also reported by Daniels (2).

6. The rule of mixtures predicts the modulus of elasticity in the axial direction very well.

7. The Halpin-Tsai and modified Halpin-Tsai equations could be used to predict the upper and lower bound value respectively for the transverse modulus of this material. The measured value was found to be in between these two values.

8. The ultimate strength of the material for off-axis

loading can be predicted by the Tsai-Hill failure criteria.

9. The Tsai-Hill failure criteria may also be used to predict the initiation of matrix cracking. The test data showed good correlation with the model except in the 30 degree off-axis loading specimen.

10. The available off-axis theories for off-axis modulus and Poissons ratio can be used to predict reasonably well for this ceramic matrix composites.

VI. Recommendations

Much has been learned about off-axis tensile loading of of ceramic composites, there remains much to be accomplished. The following areas deserve further consideration.

1. The effect of gage length on all off-axis tests conducted in this study should be investigated.
2. Additional data in the 45 degree specimen is needed to study the peculiar stress-strain relationship.
3. Off-axis testing fixture/test stand should be used to prevent bending in the specimen due to alignment limitations of the grips on the MTS machine. It should have the ability to take pictures of the crack initiation and progression while the specimen is still loaded.
4. A theory is needed to predict the beginning of matrix cracking in ceramic materials which is more precise than the Tsai-Hill failure criteria. None of the present theories anticipate the onset of matrix cracking in the linear portion of the stress-strain curve.
5. Finally, these tests should be extended to high temperature since ceramic composites are meant to be used at elevated temperatures.

Bibliography

1. Kim, Ran Y. and N. J. Pagano. "Initiation of Damage in Unidirectional Brittle Matrix Composites," Proceedings of the 4th Japan-US Conference of Composite Materials, Washington DC: 799-812 (June 1988)

2. Daniel, I. M., G. Anastassopoulos, and J-W Lee. "Failure Mechanisms in Ceramic Matrix Composites," Proceedings of the 1989 SEM Spring Conference of Experimental Mechanics, Cambridge, MA: 832-838 (1989)

3. Marshall, D. B. and A. G. Evans. "Failure Mechanisms in Ceramic-Fiber/Ceramic-Matrix Composites," Journal of the American Ceramic Society, 68, 5: 225-231 (May 1985).

4. Kim, Ran Y. and Allan P. Katz. Mechanical Behavior of Unidirectional SiC/BMAS Ceramic Composites. F33615-87-C-5239. Wright-Patterson Air Force Base, OH: Air Force Wright Aeronautical Laboratories/Materials Laboratory, 1988.

5. Jones, Robert M. Mechanics of Composite Materials. New York: Hemisphere Publishing Corporation, 1975.

6. Halpin, J. C. and S. W. Tsai. Effects of Environmental Factors on Composite Materials. AFML-TR 67-423, June, 1969.

7. Bhatt, R. T.,and R. E. Phillips. "Laminate Behavior for SiC Fiber-Reinforced Reaction-Bonded Silicon Nitride Matrix Composites," NASA Technical Memorandum 101350: (October 1988).

8. Hill, R. The Mathematical Theory of Plasticity. London: Oxford University Press, 1950.

9. Tsai, Stephen W. "Fundamental Aspects of Fiber Reinforced Plastic Composites," Strength Theories of Filamentary Structures (R. T. Schwartz and H.S. Schwartz eds). New York: Wiley Interscience, 1968.

10. Tsai, Stephen W. and Edward M. Wu. "A General Theory of Strength for Anisotropic Material," Journal of Composite Materials: 58-80 (January 1971).

11. Aveston, J., G. A. Cooper, and A. Kelly. "The Properties of Fibre Composites," Conference Proceedings, National Physical Laboratory (IPC Science and Technology Press Ltd), Paper 1: 15 (1971)

12. Aveston, J., and A. Kelly. "Theory of Multiple Fracture of Fibrous Composites," Journal of Materials Science 8: 352-362 (1973)

13. Prewo, K. M. and J. J. Brennan. "Silicon Carbide Yarn Reinforced Glass Matrix Composites," Journal of Materials Science 17: 1201-1206 (1982).

14. Brennan, J. J. and K. M. Prewo. "Silicon Carbide Fibre Reinforced Glass-Ceramic Matrix Composites Exhibiting High Strength and Toughness," Journal of Materials Science 17: 2371-2383 (1982)

Appendix

Specimen Dimensions and

Stress-Strain Curves

Table 3
Specimen Dimensions

Specimen Number	Thickness (mm)	Width (mm)	Cross Section (mm^2)	Gage Length (mm)
0-1	2.95	7.77	22.9	28.3
0-2	2.95	7.95	23.4	28.6
0-3	2.95	7.77	22.9	26.7
15-1	3.0	7.47	22.4	77.5
15-2	3.0	7.87	24.2	76.2
15-3	3.05	7.55	23.0	76.2
30-1	3.05	8.18	24.9	26.0
30-2	3.05	7.80	23.8	25.8
30-3	3.05	7.82	23.8	25.9
45-1	2.87	8.38	24.1	-
45-2	2.87	7.95	22.8	-
45-3	2.90	7.69	22.3	22.6
45-4	2.90	7.80	22.6	-
45-5	2.97	8.38	24.9	26.9
45-6	2.92	8.00	23.4	32.2
45-7	3.0	7.85	23.5	13.2
45-8	2.95	7.87	23.2	26.7
60-1	2.96	7.69	22.8	21.6
60-2	2.92	7.44	21.7	24.8
60-3	2.92	7.54	22.0	35.5
60-4	2.84	7.42	21.1	35.4
60-5	2.87	7.77	22.3	35.5
90-1	2.87	7.95	22.8	-
90-2	2.86	8.03	22.9	26.0
90-3	2.83	7.90	22.4	24.1
90-4	2.82	7.37	20.8	30.5

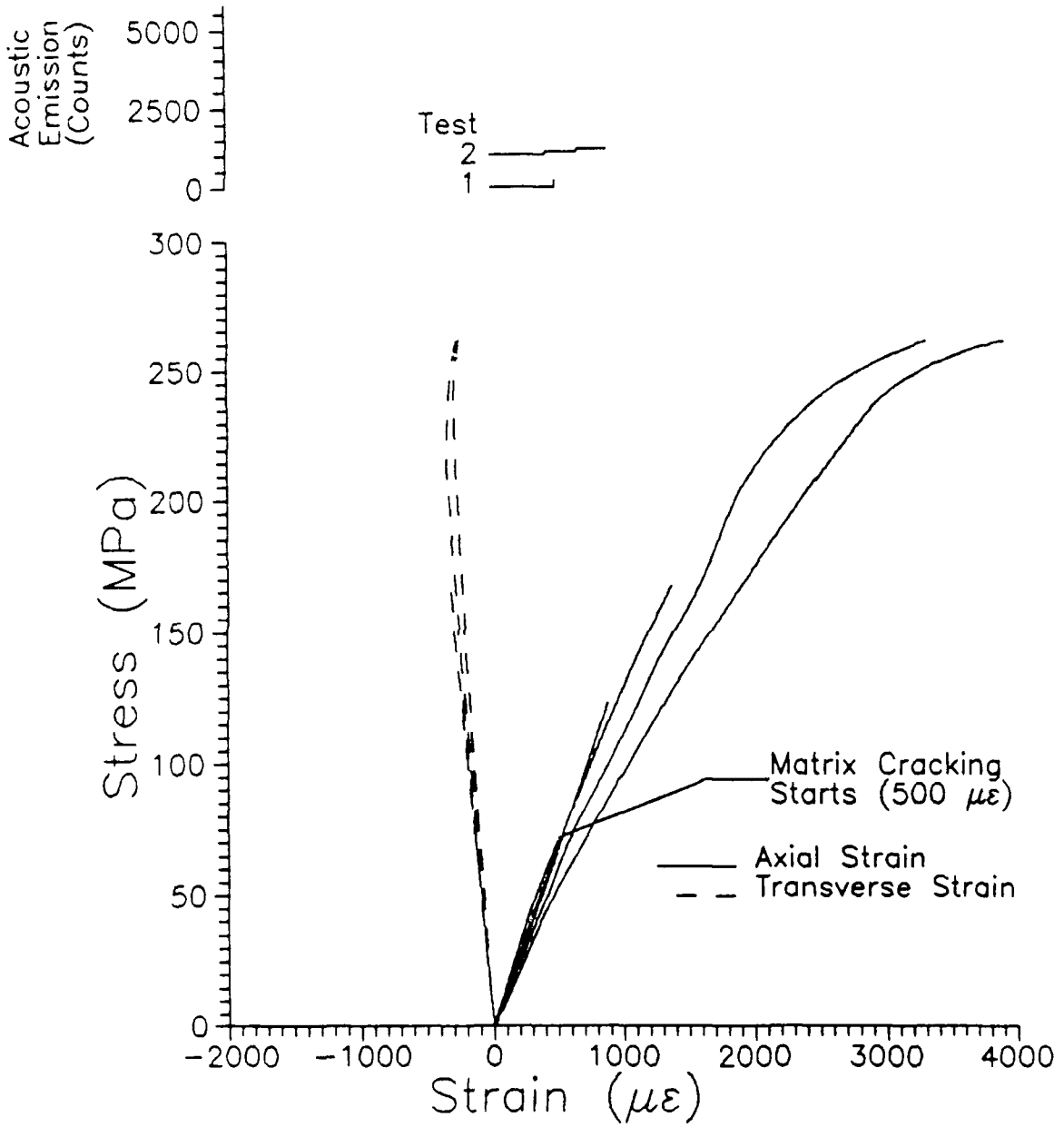

Figure 43 Stress vs Strain for 0 Degree Specimen (0-3) Incremental Loading

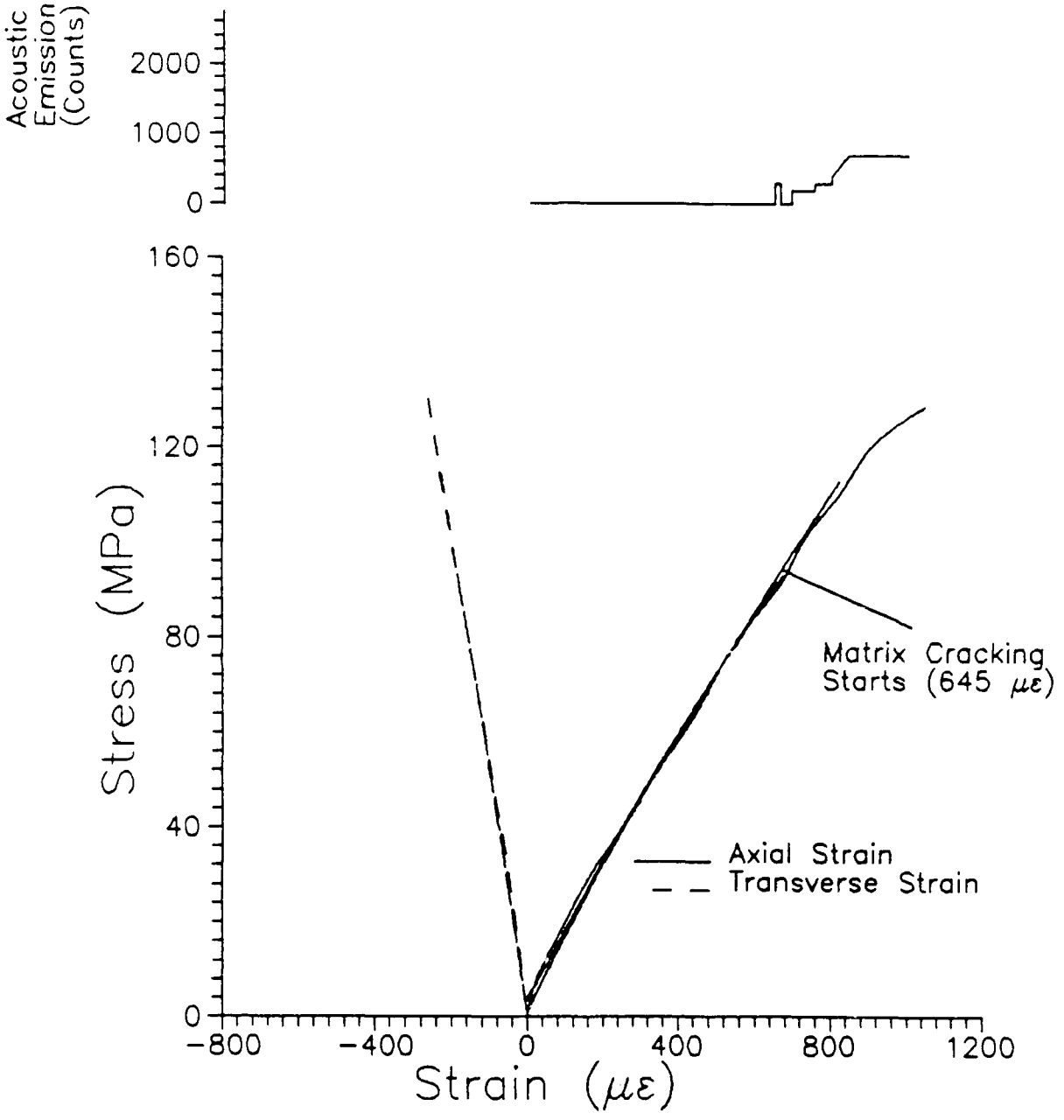

Figure 44 Stress vs Strain and Acoustic Emission for 15 Degree Specimen (15-2) Incremental Loading

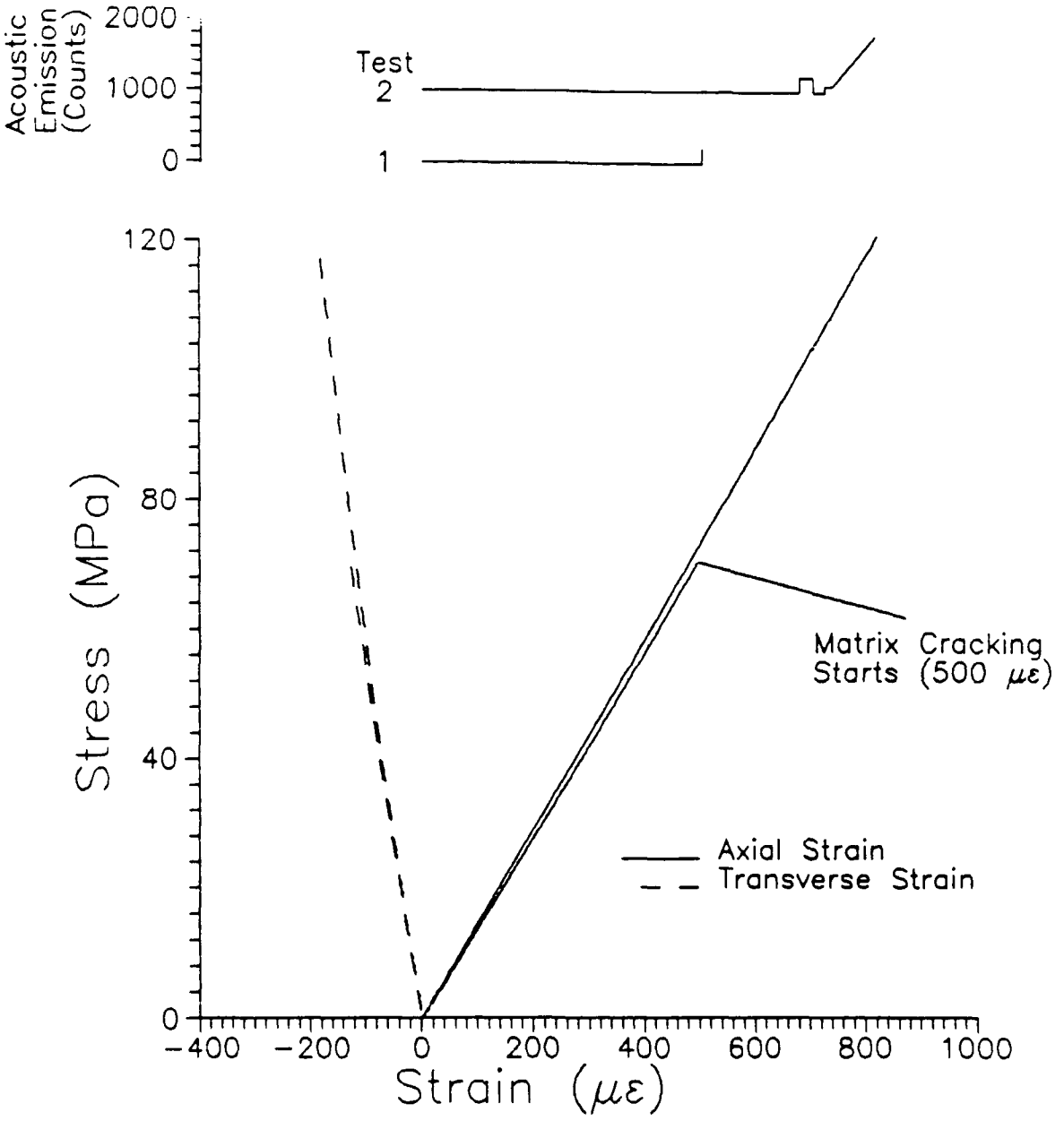

Figure 45 Stress vs Strain for 15 Degree Specimen (15-3) Incremental Loading

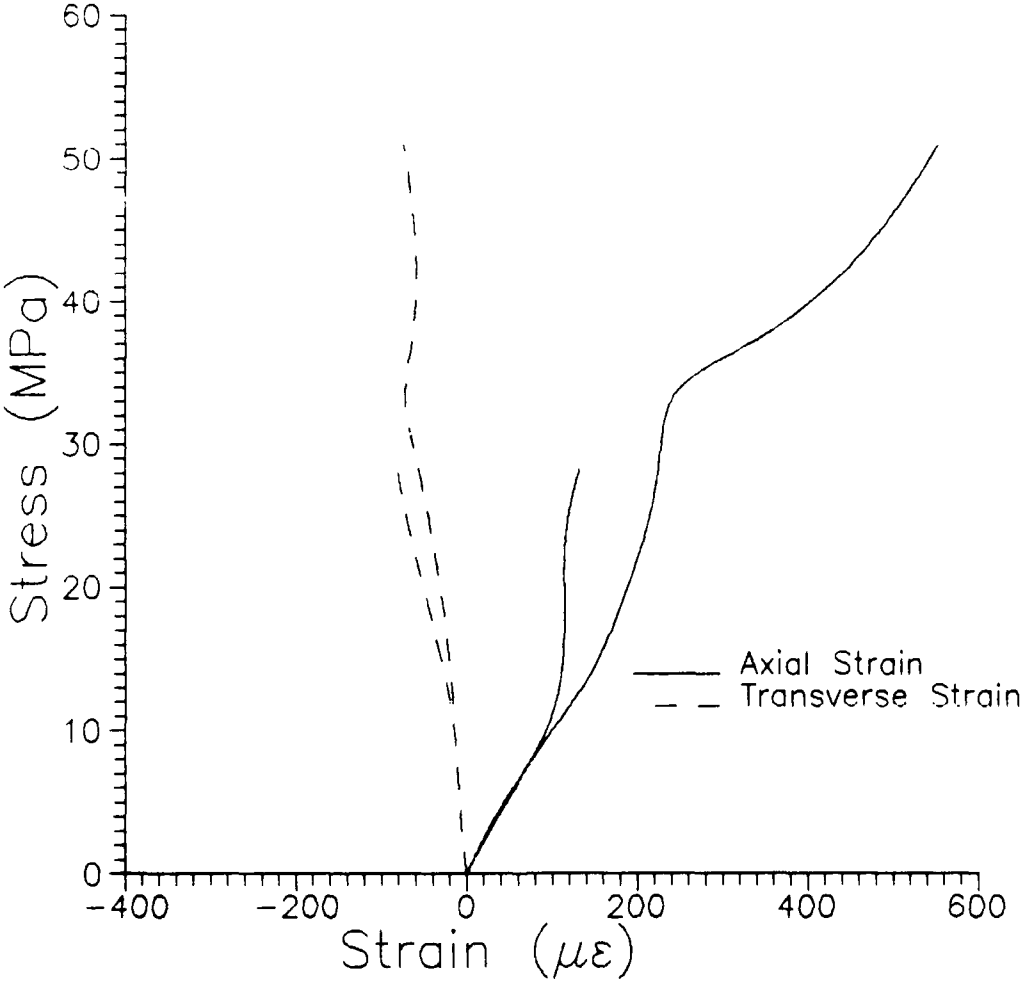

Figure 46 Nonlinear Stress vs Strain for 45 Degree Specimen (45-7) Incremental Loading

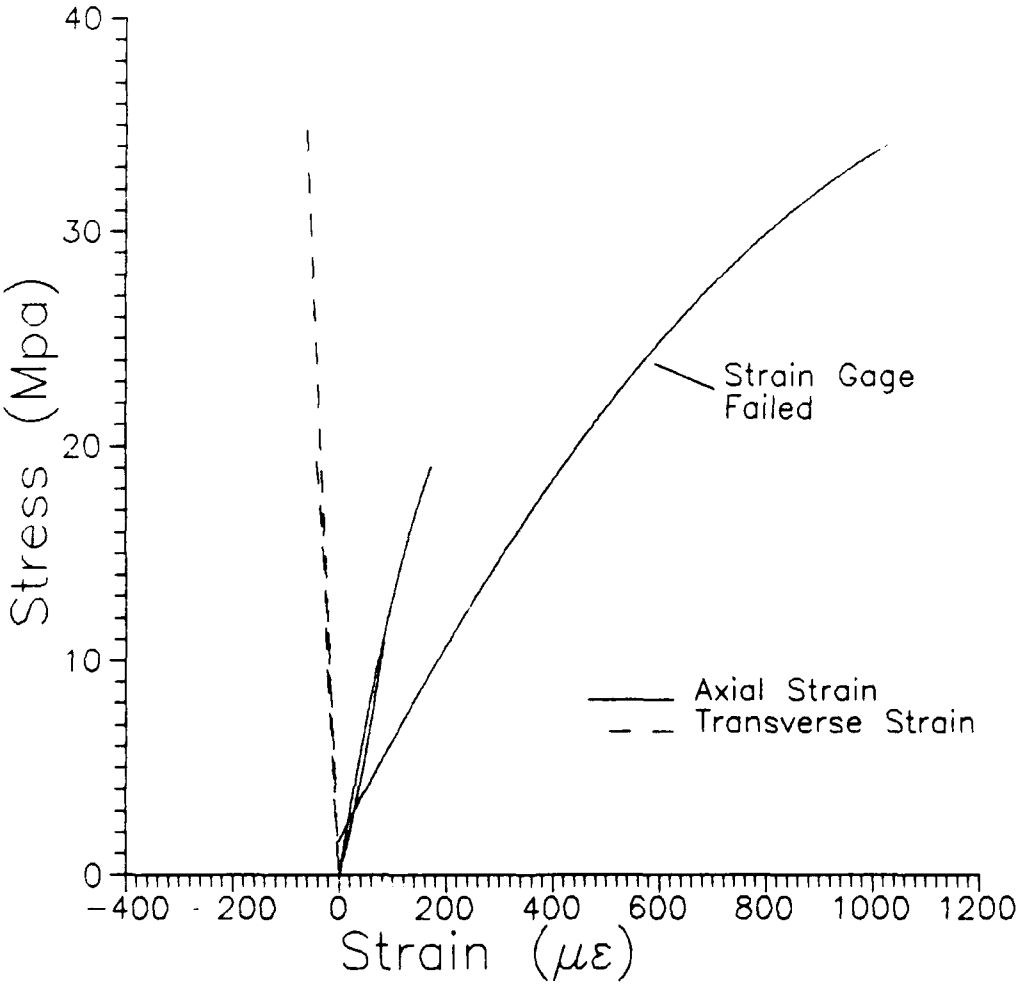

Figure 47 Stress vs Strain for 60 Degree Specimen (60-2) Incremental Loading

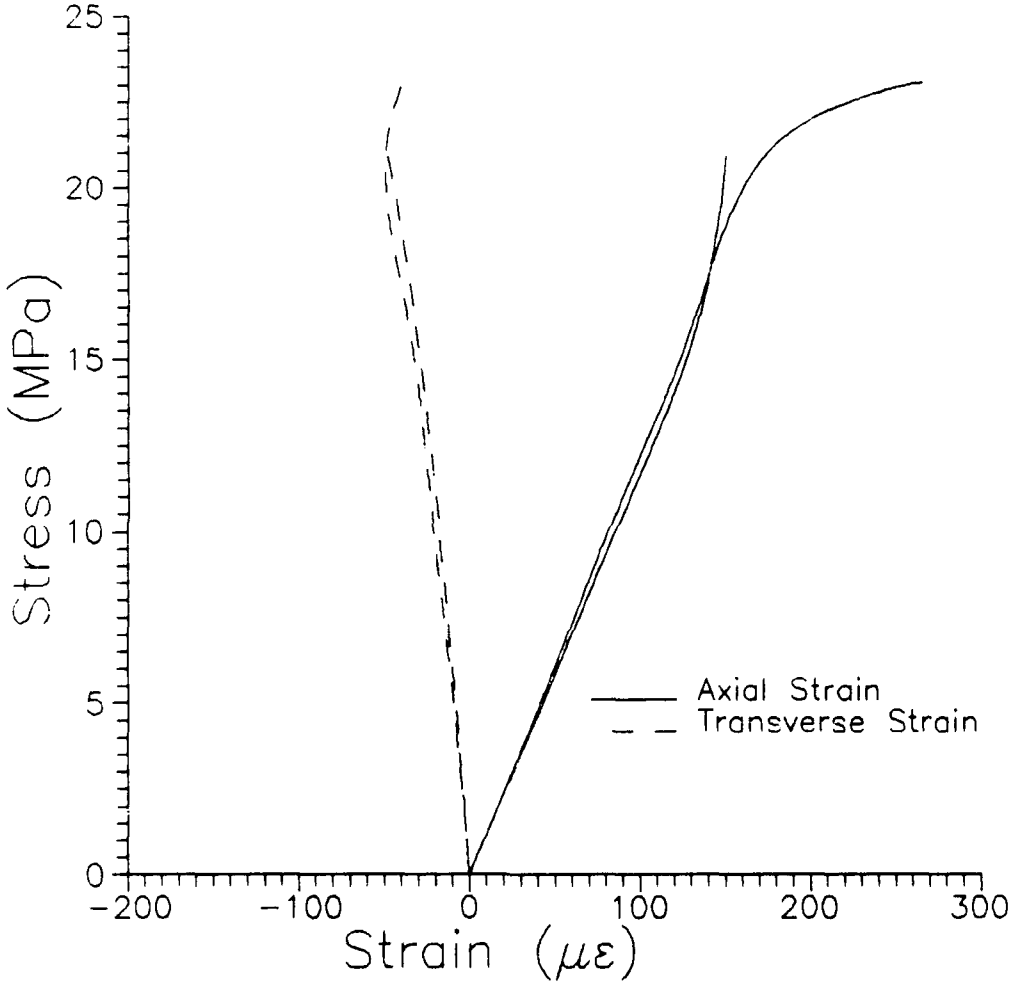

Figure 48 Stress vs Strain for 60 Degree Specimen (60-4) Incremental Loading

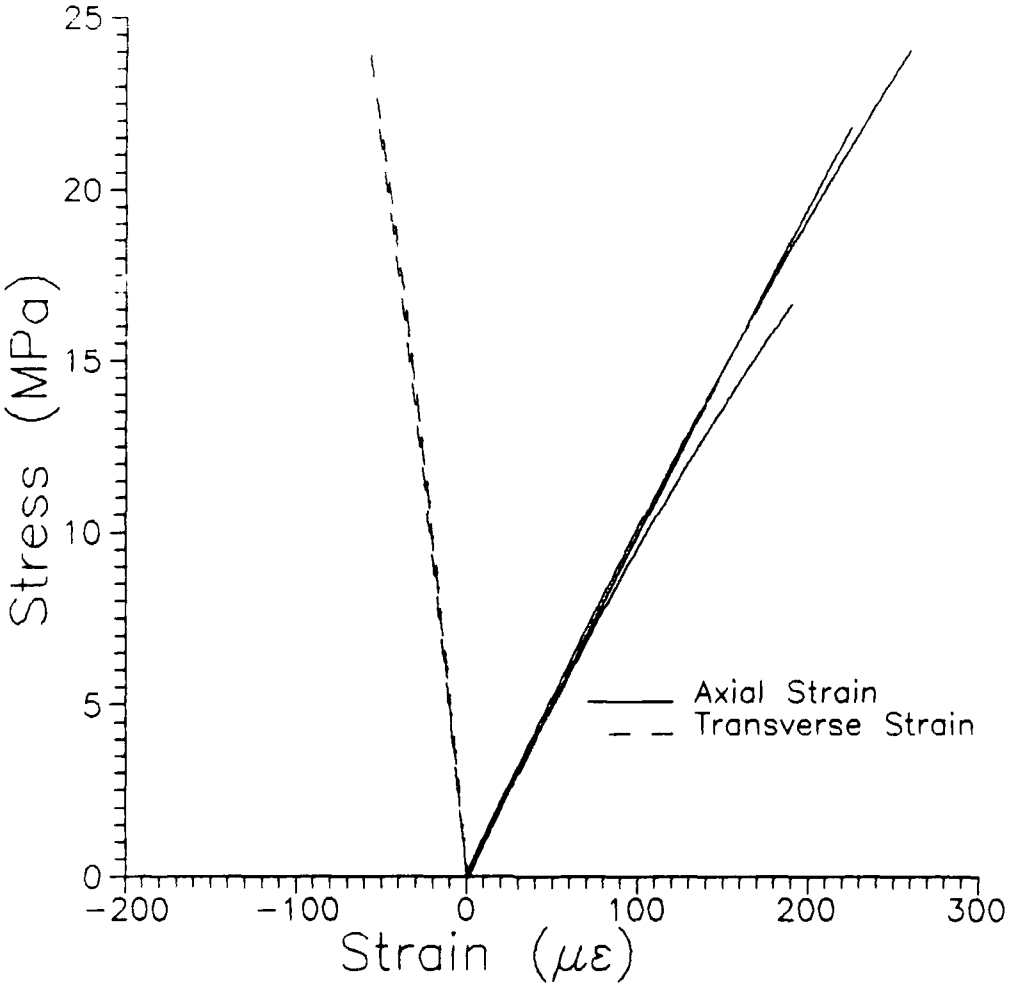

Figure 49 Stress vs Strain for 60 Degree Specimen (60-5) Incremental Loading

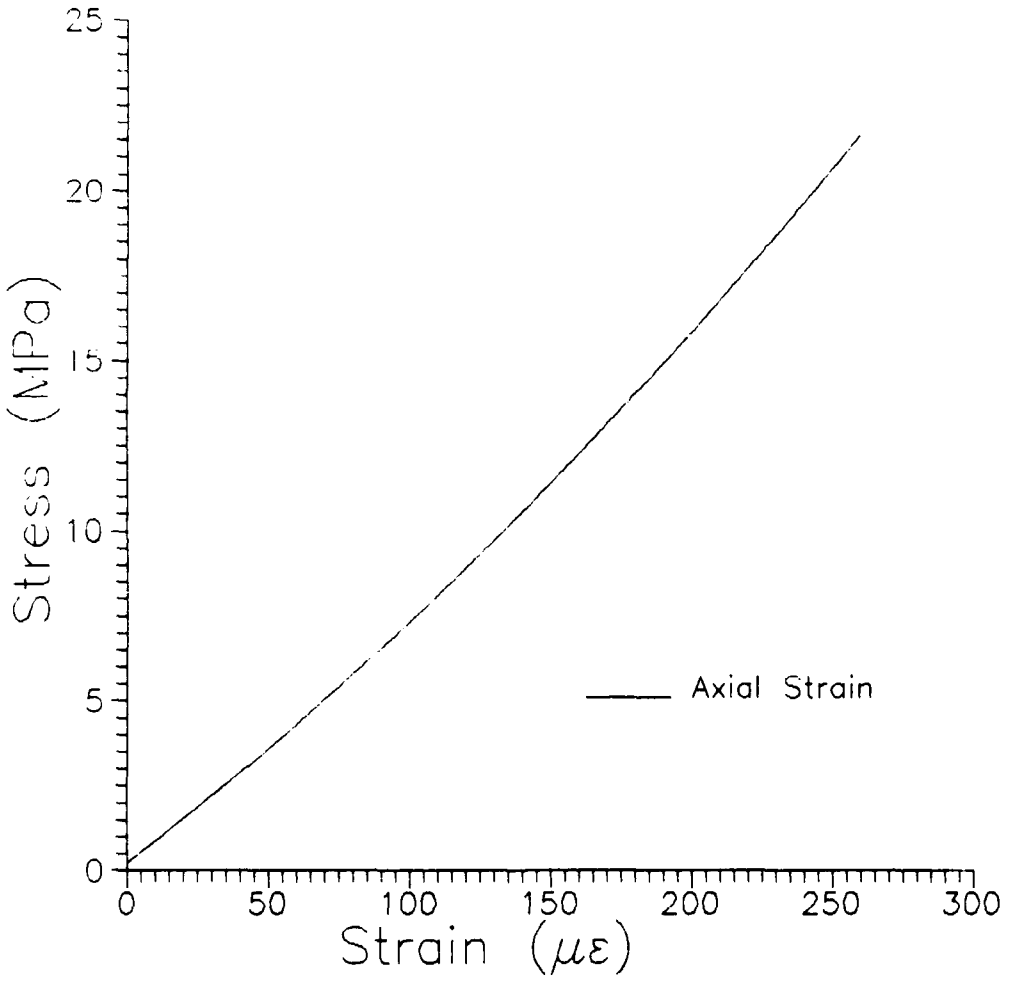

Figure 50 Stress vs Strain for 90 Degree Specimen (90-1)

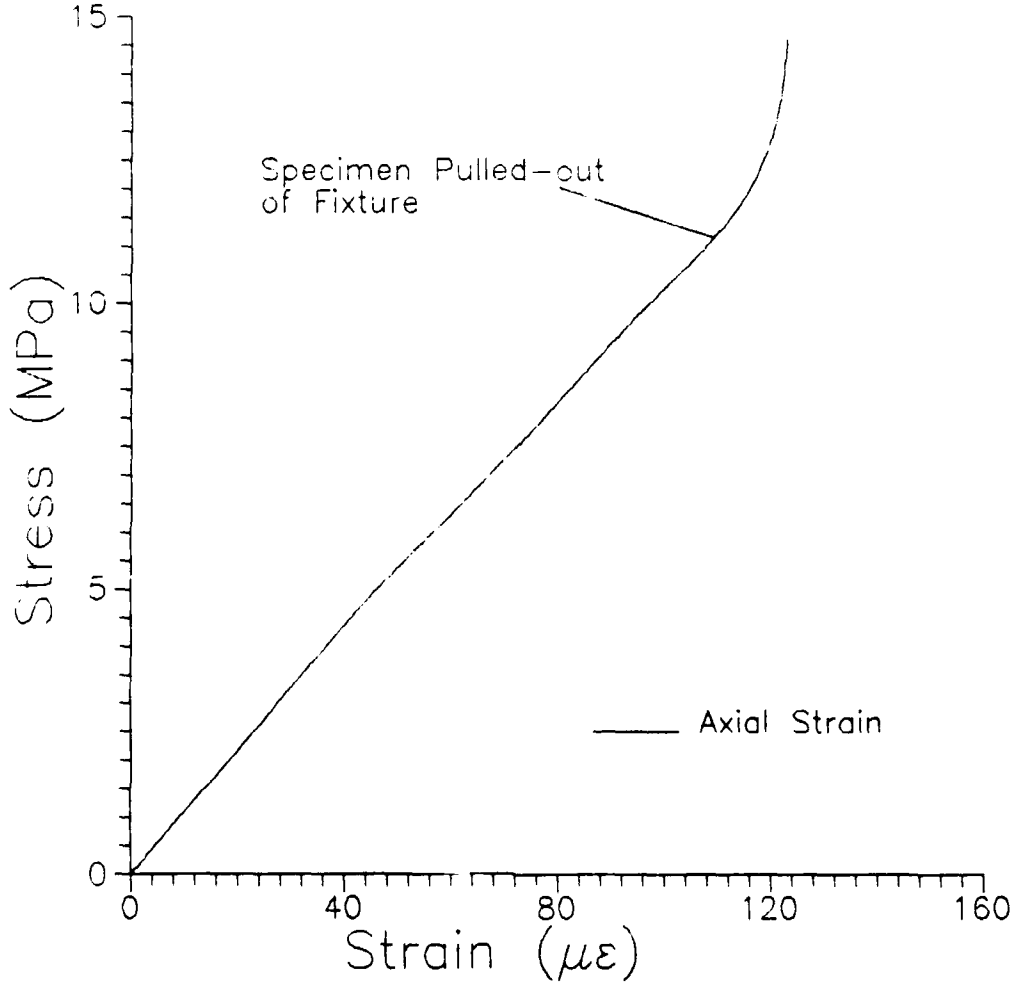

Figure 51 Stress vs Strain for 90 Degree Specimen (90-2) No Failure

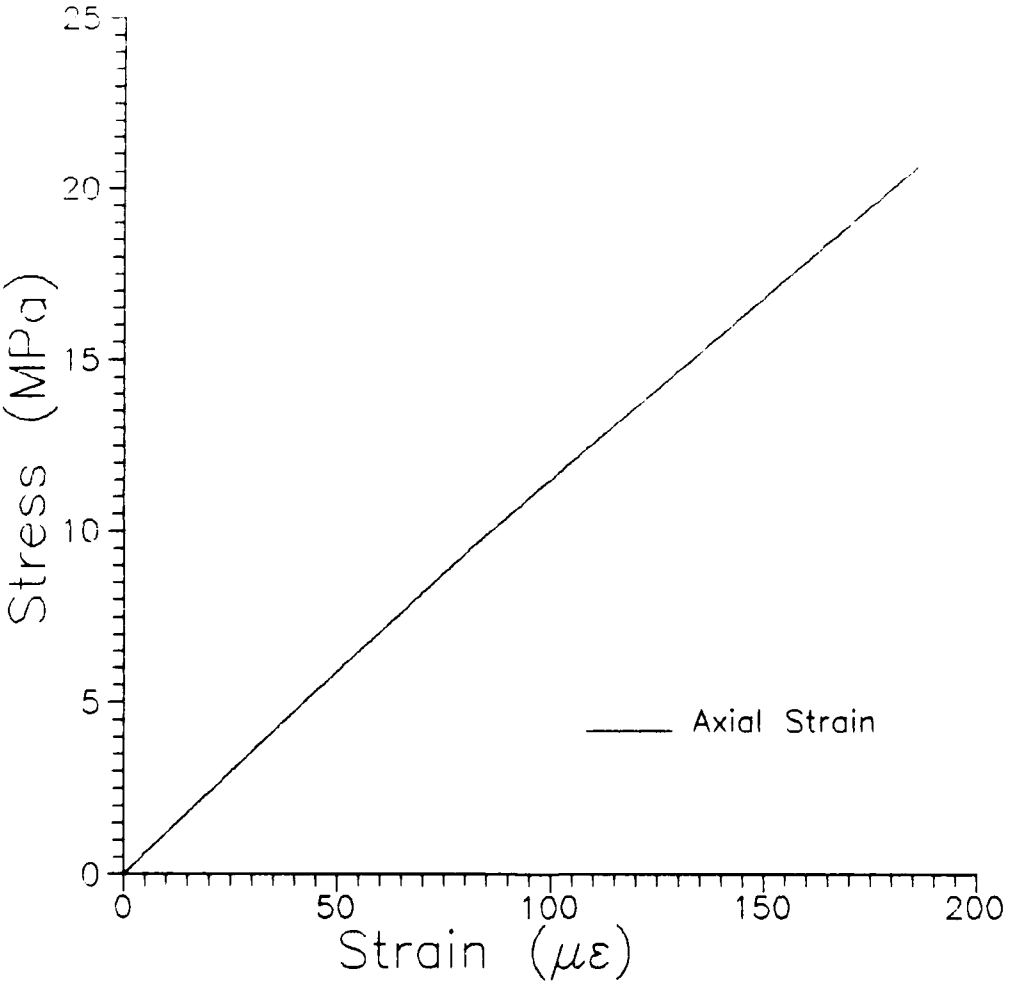

Figure 52 Stress vs Strain for 90 Degree Specimen (90-3)

Vita

Captain Walter E. Fink III [redacted] He graduated from Putnam City High School, Oklahoma City, Oklahoma in 1975. He then attended Oklahoma State University from which he received a Bachelor of Science Degree in Mechanical Engineering in December 1979. Upon graduation, he received a commission in the USAF and began his military service as the Oklahoma City Air Logistics Center Corrosion Program Manager at Tinker AFB, Oklahoma. Then he served as a reliability and maintainability engineer for the Common Strategic Rotary Launcher and B-2 Operational Test and Evaluation Test Teams at Edwards AFB, California. He then entered the School of Engineering, Air Force Institute of Technology in May 1988.

[redacted]

UNCLASSIFIED
SECURITY CLASSIFICATION OF THIS PAGE

REPORT DOCUMENTATION PAGE

Form Approved
OMB No. 0704-0188

1a. REPORT SECURITY CLASSIFICATION UNCLASSIFIED	1b. RESTRICTIVE MARKINGS
2a. SECURITY CLASSIFICATION AUTHORITY	3. DISTRIBUTION/AVAILABILITY OF REPORT Approved for public release; distribution unlimited
2b. DECLASSIFICATION/DOWNGRADING SCHEDULE	
4. PERFORMING ORGANIZATION REPORT NUMBER(S) AFIT/GAE/ENY/89D-9	5. MONITORING ORGANIZATION REPORT NUMBER(S)
6a. NAME OF PERFORMING ORGANIZATION School of Engineering 6b. OFFICE SYMBOL (If applicable) AFIT/ENY	7a. NAME OF MONITORING ORGANIZATION
6c. ADDRESS (City, State, and ZIP Code) Air Force Institute of Technology Wright-Patterson AFB OH 45433-6583	7b. ADDRESS (City, State, and ZIP Code)
8a. NAME OF FUNDING/SPONSORING ORGANIZATION 8b. OFFICE SYMBOL (If applicable)	9. PROCUREMENT INSTRUMENT IDENTIFICATION NUMBER
8c. ADDRESS (City, State, and ZIP Code)	10. SOURCE OF FUNDING NUMBERS PROGRAM ELEMENT NO. / PROJECT NO. / TASK NO / WORK UNIT ACCESSION NO

11. TITLE (Include Security Classification)
Investigation of Failure Modes in Ceramic Composites under Off-axis Loading

12. PERSONAL AUTHOR(S)
Walter E. Fink III, B.S., Capt, USAF

13a. TYPE OF REPORT	13b. TIME COVERED	14. DATE OF REPORT (Year, Month, Day)	15. PAGE COUNT
MS Thesis	FROM _____ TO _____	1989, December	119

16. SUPPLEMENTARY NOTATION

17. COSATI CODES			18. SUBJECT TERMS (Continue on reverse if necessary and identify by block number)
FIELD	GROUP	SUB-GROUP	Fiber Reinforced Composites, Ceramic Composite, Off-axis loading
11	02		

19. ABSTRACT (Continue on reverse if necessary and identify by block number)

Thesis Advisor: Dr. Shankar Mall
Professor
Department of Aeronautics and Astronautics

Abstract on Reverse

20. DISTRIBUTION/AVAILABILITY OF ABSTRACT	21. ABSTRACT SECURITY CLASSIFICATION
☒ UNCLASSIFIED/UNLIMITED ☐ SAME AS RPT ☐ DTIC USERS	UNCLASSIFIED

22a. NAME OF RESPONSIBLE INDIVIDUAL	22b. TELEPHONE (Include Area Code)	22c. OFFICE SYMBOL
Dr. Shankar Mall, Professor	(513) 255-2998	AFIT/ENY

DD Form 1473, JUN 86 *Previous editions are obsolete.*

SECURITY CLASSIFICATION OF THIS PAGE
UNCLASSIFIED

The purpose of this study was to investigate the failure behavior of a ceramic composite (Corning's Nicalon/CAS II) under off-axis loading, and compare the test results with material behavior modeling techniques for polymeric composites.

Six different orientations (0, 15, 30, 45, 60, and 90 degrees off axis), with three specimens at each orientation, were tested in an MTS machine. The 60 and 90 degree specimens were tested by gluing them into a fixture that had already been installed into the grips. All others were install in the grips. At least one specimen of each orientation was tested to its ultimate failure. Thereafter, other specimens were tested incrementally, stopping along the way, to find when and where matrix cracking starts. Acoustic emission was used to determine when cracking starts and replication was used to confirm the cracking.

The 0, and 15 degree specimens started cracking in the matrix during the linear portion of the stress-strain curve, at about 35 percent of their ultimate strengths. The rest of the orientations cracked when they reached the ultimate strength. All off-axis load orientations broke parallel to the direction of the fiber, except the 15 degree which was 25 degrees off-axis. The 0 degree specimen showed a decrease in transverse strain before final failure occurred.

The test results showed that the Tsai-Hill failure criteria can approximate the ultimate failure stress and matrix cracking stress for this material in off-axis loading. The present modeling techniques for E_x and ν_{xy} will predict a trend for these values for this material. The average values of E_x and ν_{xy} were close to the predicted values. The measured E_1 was in good agreement with its predicted value using the rule of mixtures. But E_2 was found to be in between the values obtained from the Halpin-Tsai equation (assuming a strong bond between the fiber and matrix) and the modified Halpin-Tsai equation (assuming no bond).